TECHNICAL DISCLOSURE 02

Integrated Orbital Propellant Aggregation Architecture for Cryogenic Tanker-to-Depot Campaigns at Starship Scale

Integrated suppression of boil-off, zero-gravity liquid acquisition failure, slosh at transfer transients, zero-gravity mass-gauging error, cryogenic docking attrition, and mated-stack attitude coupling

FILER	Coracle Research
PUBLICATION DATE	21 April 2026
PRIMARY VENUE	coracleresearch.com/research/02-starship-refilling/disclosure.html
PREPRINT DEPOSIT	Zenodo, DOI 10.5281/zenodo.19701811; additional mirror on engrXiv pending moderation
LEGAL STATUS	Defensive publication under 35 U.S.C. §102
COMPANION	Research Note 02: Tanker aggregation and the Starship propellant horizon

The subject matter of this disclosure is an integrated ship-to-ship cryogenic-propellant aggregation architecture for a Starship-class fully reusable launch vehicle, addressing, in a single operational system and across a multi-flight aggregation campaign, six concurrent cryogenic fluid-management challenges: passive plus active suppression of propellant boil-off across a multi-week low-Earth-orbit hold; zero-gravity acquisition of liquid cryogen at the tank outlet across continuous and start-stop flow regimes; slosh mitigation across the transfer-duration-scale fundamental mode at coast-gravity conditions; mass gauging to sub-one-percent aggregate accuracy across

multi-transfer campaign durations; cryogenic androgynous berthing with fluid-transfer interface meeting fleet-scale mate-demate cycle life; and attitude control of the mated-tandem stack across live mass transfer and a continuously drifting center of mass. The architecture comprises six coordinated subsystems with specified composition windows, power budgets, component specifications, and operations sequences. Alternative embodiments, a worked example at a fifteen-flight aggregation campaign, enablement specifications, and numbered figures are given below. This document is published as prior art under 35 U.S.C. §102 for defensive purposes as of the publication date above.

§ 1

Title and Filer

The invention disclosed herein is titled *Integrated Orbital Propellant Aggregation Architecture for Cryogenic Tanker-to-Depot Campaigns at Starship Scale, Providing Integrated Suppression of Boil-off, Zero-Gravity Liquid Acquisition Failure, Slosh at Transfer Transients, Zero-Gravity Mass-Gauging Error, Cryogenic Docking Attrition, and Mated-Stack Attitude Coupling*. The filer of record is Coracle Research. The effective publication date is the date stated in the masthead and in the filer block above. A preprint copy of this disclosure is deposited on Zenodo under DOI 10.5281/zenodo.19701811 for examiner-searchable durability, with an additional mirror on engrXiv pending moderation, and a PDF paper copy is available for download from the primary venue. A companion narrative research note, referenced above, describes the same subject matter in a more accessible register.

§ 2

Field of the Invention

The invention relates to in-space cryogenic fluid management, and more particularly to ship-to-ship orbital propellant transfer and aggregation architectures for fully reusable two-stage-to-orbit launch vehicles operating on liquid methane and liquid oxygen at propellant loads in the range 1000 to 2000 metric tons per vehicle. The architecture is specified for a Starship-class vehicle with tank geometry in the range 8 to 10 meters interior diameter and 20 to 35 meters propellant-compartment length per tank, operating in low Earth orbit at altitudes of 300 to 600 kilometers, with propellant aggregation campaigns in the range 4 to more than 20 tanker flights per receiver and aggregation hold durations in the range 7 to 60 days. The invention addresses the integrated management of six concurrent cryogenic-fluid-management mechanisms whose simultaneous action determines the feasibility of any orbital-refilling-dependent mission architecture, including but not limited to Mars transfer, lunar transfer with high departure-mass margin, and in-space depot operations for third-party vehicles.

§ 3

Background and Prior Art

Six cryogenic fluid-management mechanisms are known in the published space-systems-engineering literature to constrain the feasibility of orbital propellant transfer and aggregation at thousand-ton scale on methalox-class vehicles in low Earth orbit.

Boil-off. Cryogenic propellants stored in orbit absorb radiative heat from direct solar flux, Earth albedo and infrared emission, and internal dissipation sources. Absorbed heat vaporizes propellant at a rate set by the heat load divided by the latent heat of vaporization. On a bare polished stainless tank surface at central solar-optical values (solar absorptance $\alpha_s = 0.35$, infrared emittance $\varepsilon_{IR} = 0.12$), the absorbed flux is approximately 137 watts per square meter orbit-averaged, driving boil-off rates of approximately 2.5 to 3 percent per day for Starship-class methalox tanks at central assumptions and rising to approximately 4.5 percent per day in aged-skin cases. The physical basis and operational consequences are reviewed in Simonini et al., *npj Microgravity* 10, 34 (2024), and in Barron, *Cryogenic Heat Transfer*, 2nd ed., CRC Press (2016). Heritage cryogenic-storage-testing programs including SHIIVER (NTRS 20205008233), MHTB (NTRS 20110009964, 20100034929), and CRYOTE (NTRS 20090037680) have characterized multilayer-insulation performance on representative propellant tanks, with published residual-heat-flux benchmarks near 1 watt per square meter after installation. Zero-boil-off cryocooler architectures have been characterized at laboratory scale by NASA Glenn Research Center (Plachta and Kittel, NTRS 20030067928; Hedayat et al., NTRS 20020017748; Johnson, NTRS 20170001537; Plachta and Hartwig, NTRS 20180004709).

Zero-gravity liquid acquisition. In the absence of gravitational settling, liquid propellant in a partially filled tank is positioned by surface tension and by residual acceleration. Surface tension forces at cryogenic temperatures (methane surface tension 13.3 millinewtons per meter at normal boiling point; LOX surface tension 13.2 millinewtons per meter) are weak relative to inertial forces at tank radii of 4 to 5 meters. The Bond number $Bo = \rho g R^2/\sigma$ computed on tank radius ($R = 4.5$ m), surface tension, and typical residual acceleration of 10^{-5} g is approximately 63 for liquid methane and 172 for liquid oxygen at Starship-scale geometry, both well into the inertial-force-dominated regime ($Bo \gg 1$), placing passive surface-tension positioning of bulk liquid outside the feasible operating regime. Heritage propellant-management-device (PMD) architectures at smaller scales are reviewed in NASA SP-106 (Abramson 1966), and modern cryogenic propellant positioning by hybrid PMD-plus-settling approaches is reviewed in Hartwig, *Liquid Acquisition Devices for Advanced In-Space Cryogenic Propulsion Systems*, Academic Press (2016). Recent work on modeling cryogenic transfer in microgravity is given in Kassemi et al., *npj Microgravity* 10, 51 (2024), and in the SpaceX-co-authored two-phase-flow paper NTRS 20250003325 (2025).

Slosh at transfer transients. Propellant mass in a partially filled tank responds to imposed accelerations and to flow-rate transients by exciting natural modes of sloshing. The fundamental lateral slosh mode of a cylindrical tank at deep fill has a period that scales with the square root of effective gravity (Abramson, NASA SP-106, 1966). At 9-meter tank radius under coast-gravity conditions at 10^{-5} g, the first lateral-mode period exceeds 16 minutes, comparable to full transfer durations. At elevated settling thrust of 10^{-3} g, the period drops below 2 minutes, within the bandwidth of standard attitude-control-system damping.

Zero-gravity mass gauging. The mass of cryogenic propellant in a zero-gravity tank cannot be measured by surface-height methods. Candidate methods include pressure-volume-temperature (PVT) gauging, radio-frequency (RF) tank-level measurement, compression gauging, fiber-optic distributed-temperature sensing (DTS), and multi-sensor fusion. Flight experience is limited: RF mass gauging flew on the Intuitive Machines Nova-C lunar lander in February 2024 with published accuracy reports in the 1 to 3 percent range for the Nova-C scale (NTRS 20240014338). Underlying measurement-method theory is given in Zimmerli et al. (NTRS 20070031548) and in NASA guidelines document NTRS 20250004625 (2025). Published ground-test accuracies for DTS on cryogenic tanks range from 0.5 to 2 percent under controlled conditions.

Cryogenic androgynous docking with fluid transfer. Orbital fluid transfer between two free-flying spacecraft has been demonstrated once, during the DARPA Orbital Express mission of March to July 2007, which transferred approximately 14 kilograms of hydrazine across four autonomous mate-demate cycles (Rotenberger et al., Proc. SPIE 6958, 695808, 2008). Orbital Express used storable hydrazine at ambient temperature and did not address cryogenic-temperature seal life, cryogenic-interface thermal shock, or repeated-cycle wear at flight-fleet scale. Heritage cryogenic ground-fitting architectures including the Johnston coupler, quick-disconnect fittings for liquid helium and liquid nitrogen transfer, and the CBM and NDS orbital docking mechanism families provide separate precedents for seal design and for mechanical-capture geometry but not for the integrated combination at Starship scale.

Mated-stack attitude coupling. Two spacecraft mated along a common axis form a combined system whose dynamics are governed by the combined moment of inertia, by the instantaneous center-of-mass position, and by any time-varying coupling between internal fluid motion and rigid-body motion. A mated Starship pair at Block 2 geometry (approximately 104 meters total length) exhibits a combined moment of inertia, computed under uniform-rod approximation on the mated stack, that varies with mated-stack mass across the aggregation campaign, from approximately 3.9×10^8 kilogram square meters at transfer 1 (mated mass approximately 430 metric tons, receiver near-empty) to approximately 1.67×10^9 kilogram square meters at transfer 15 (mated mass approximately 1830 metric tons, receiver near-full). Continuous mass transfer between vehicles during each 20-to-40-minute transfer interval drives per-transfer center-of-mass shifts of approximately 3 to 12 meters along the mated-stack axis depending on aggregation state. Heritage spacecraft attitude-control-system design is reviewed in Wie, *Space Vehicle Dynamics and Control*, 2nd ed., AIAA (2008). Model-predictive control for spacecraft dynamics with internal slosh states has been demonstrated in ground hardware-in-loop testing but not at Starship operational scale.

Individual prior-art interventions against each of the six mechanisms have been published. No publication known to the filer combines all six interventions into a single integrated aggregation architecture specified at Starship scale (1000-ton-class propellant loads, 10-plus-flight aggregation campaigns, 104-meter mated-stack attitude coupling with live mass flow). The most relevant prior art is enumerated below.

[1] G. Grayson, M. Hand, E. Cady (Boeing), "Thermally coupled liquid oxygen and liquid methane storage vessel with shared cryocooler and vapor-cooled shield," U.S. Patent 7,568,352 B2, filed 2006, granted 2009. Discloses a combined LO2/LCH4 storage vessel with liquid acquisition devices in each tank, a thermal-vapor-shield cooling scheme with a cryocooler on the LOX side conducting to the methane side, and a vapor-cooled shield surrounding the combined assembly. The closest two-cryogen thermal-stack precedent. Disclosed at single-vehicle concept scale (upper-stage or standalone depot) and contemplates use as an "orbital depot" but does not disclose ship-to-ship fluid transfer to a separate receiver vehicle, does not disclose mated-tandem attitude coupling, and does not disclose multi-flight aggregation operations.

[2] G. Grayson and E. Cady (Boeing), "Thermally protected liquid acquisition device for cryogenic fluids," U.S. Patent 9,395,048 B1, filed 2010, granted 2016. Discloses an in-tank cryogenic LAD spaced from the tank wall, with integrated spray injection, primary and secondary heat exchangers, thermal destratification, and pressure and temperature control. Directed to single-tank intra-vehicle liquid acquisition. Does not disclose hybrid PMD-plus-settling operation, does not disclose Starship-scale (9-meter-diameter) tank geometry, and does not disclose ship-to-ship transfer operations.

[3] B. Kutter, F. Zegler, C. Willey, J. Lin, M. Ragab, M. Dew (United Launch Alliance), "Cryogenic propellant depot and deployable sunshield," U.S. Patent 8,196,869 B2, priority 2009, granted 2012. Discloses a dedicated orbital propellant depot with a deployable sunshield providing solar-flux reduction, differential-pressure tank-to-tank transfer, and axial rotation of the depot about its longitudinal axis to centrifugally position a gaseous ullage at the tank center. Claims the rotation-based centrifugal acquisition as both an apparatus (claim 1) and method (claim 14). Directed to a single-vehicle depot at substantially smaller scale than Starship (Centaur-class upper-stage derivation). Does not disclose ship-to-ship transfer to a receiver vehicle, does not disclose mated-tandem operations, does not disclose active 10^{-3} g settling-thrust-driven acquisition as an alternative to rotation, and does not disclose the six-subsystem integrated architecture.

[4] A. Allen, J. Lymer, K. Spring, R. Ravindran (MacDonald Dettwiler), "Propellant transfer system and method for resupply of fluid propellant to on-orbit spacecraft," U.S. Patent 9,260,206 B2, priority 2011, granted 2016. Direct descendant of the Orbital Express storable-fluid transfer architecture. Directed to servicer-to-client fluid transfer of storable propellants (hydrazine, MMH, UDMH, MON3). Does not disclose cryogenic-temperature operations, does not disclose thousand-ton-class propellant volumes, and does not disclose multi-transfer aggregation campaigns.

[5] F. Zegler (United Launch Alliance), "Integrated vehicle fluids," U.S. Patent 10,717,550 B1, filed 27 October 2017, granted 21 July 2020. Discloses a stage-integrated internal-combustion engine powered by ullage-gas cryogen boil-off for electric power and for settling-thrust generation from autogenous warm-gas venting. Relevant precedent for warm-gas autogenous settling thrust (RCS architecture on which Component B duty-cycled coast-settling draws). Does not disclose ship-to-ship transfer and does not disclose a Starship-scale integrated aggregation architecture.

[6] Altius Space Machines Inc. (Voyager Technologies), cryogenic electro-permanent-magnet (EPM) coupler family, U.S. patent application pending per company statement (2020-2025); cryogenic fluid-transfer coupling delivered under NASA SBIR Phase II (contract 80NSSC19C0088) and integrated into the Eta Space LOXSAT mission (launched 2026). Discloses a cryogenic androgynous fluid-transfer coupling using EPM latching for low-connection-force mechanical capture. Closest mechanical-capture precedent for Component E (cryogenic docking subsystem). Does not disclose autogenous-methane condensation as a secondary leak barrier, does not disclose Starship-scale (150-to-250-mm transfer-line diameter) fluid-transfer flow rates, and does not disclose the six-subsystem integrated architecture.

[7] A. Weiss, D. Zlotnik, S. Di Cairano (Mitsubishi Electric Research Laboratories), "Model predictive control of spacecraft," U.S. Patent 10,967,991 B2, filed 10 August 2017, granted 6 April 2021. Discloses model-predictive control for single-spacecraft station-keeping, attitude, and momentum management. Relevant precedent for Component F (attitude coupling controller). Does not disclose mated-tandem vehicle dynamics, does not disclose real-time moment-of-inertia tracking under continuous inter-vehicle mass transfer, does not disclose mass-flow-rate feedforward, and does not disclose augmentation of slosh-mode state variables in the MPC state vector at the scale disclosed herein.

[8] NASA Kennedy Space Center, "Low Separation Force Quick Disconnect" (KSC-TOPS-63), NASA Technology Transfer Portal, published August 2022. Discloses a cryogenic quick-disconnect fitting with low separation force at mate and demate, using government-licensed IP. Supporting state-of-art for Component E cryogenic fitting architecture.

[9] G. Zimmerli and M. Vaden (NASA), "Radio frequency mass gauging of propellants," NTRS 20070031548, 2007, and "Results from the Radio Frequency Mass Gauge Technology Demonstration on the IM Nova-C Lunar Lander," NTRS 20240014338, 2024. Discloses RF tank-level mass gauging and reports flight performance at Nova-C scale. Single-method, single-tank architecture. Does not disclose multi-sensor fusion with DTS and PVT cross-check, and does not disclose Starship-scale measurement-error aggregation across 10-plus transfers.

[10] S. Rotenberger, D. SooHoo, G. Abraham (Northrop Grumman Corp.), "Orbital Express fluid transfer demonstration system," Proc. SPIE 6958, 695808 (15 April 2008), DOI 10.1117/12.783948. Discloses the Orbital Express demonstration architecture for storable-propellant autonomous transfer. Used hydrazine at ambient temperature. Does not address cryogenic seal life, does not address thermal shock at mate, and does not address repeated-cycle fleet-scale operations.

[11] D. Plachta, J. Hartwig, et al. (NASA Glenn), "NASA cryocooler technology developments and goals to achieve zero boil-off and to liquefy cryogenic propellants for space exploration," NTRS 20180004709 (2018), and prior family including NTRS 20030067928, 20020017748, 20170001537. Discloses cryocooler performance, MLI-plus-cryocooler architectures, and ZBO power budgets at laboratory and sub-propellant-tank scale. Does not address ship-to-ship transfer, does not address integrated six-subsystem operation, and is directed to component-level research programs without integrated operational architecture coverage.

[12] NASA, "Guidelines for In-Space Cryogenic Propellant Transfer (ISCPT)," NASA MSFC Cryogenic Fluid Management Portfolio Project, April 2025 (NTRS 20250004625; AIAA ASCEND 2025-4122). Government-authored engineering-guidance document for in-space cryogenic transfer covering several of the mechanisms described herein at advisory level. Does not commit to specific architectural choices and is not a patent filing.

[13] H. Tani, L. Blackmore, G. Thome (SpaceX), "In-Space Cryogenic Propellant Transfer: Modeling and Validation of Two-Phase Flow Dynamics in Low-Gravity," NTRS 20250003325 (April 2025). SpaceX-authored analytical-modeling paper on two-phase flow in cryogenic transfer. Directed to fluid-dynamic modeling methodology. No corresponding patent filing. Consistent with a posture of trade-secret protection on the integrated operational architecture.

[14] Simonini, Dreyer, Urbano et al., "Cryogenic propellant management in space: open challenges and perspectives," *npj Microgravity* 10, 34 (2024). Published review of the field at the time of the present disclosure. Notes explicitly that ship-to-ship cryogenic transfer between independent spacecraft has never been demonstrated at scale, and that Starship-scale aggregation is an open problem.

[15] M. Kassemi, A. Hylton et al., "Demonstration of charge-hold-vent and no-vent-fill in a simulated propellant storage tank during tank-to-tank cryogen transfer in microgravity," *npj Microgravity* 10, 51 (2024). Reports in-flight charge-hold-vent and no-vent-fill demonstrations at small scale.

[16] H. N. Abramson, "The dynamic behavior of liquids in moving containers," NASA SP-106 (1966). Foundational reference for tank-slosh dynamics.

[17] NASA Office of Inspector General, "NASA's Management of the Human Landing System Contracts," IG-26-004, March 2026. Programmatic-review document noting that Starship ship-to-ship cryogenic transfer remains unflown as of the report date and is an open critical-path item for Artemis III; reports "more than 10" tanker flights per HLS mission with SpaceX targeting a one-tanker-per-6-days cadence.

[18] Standard optical-property data for polished 300-series stainless steel in space environment, including NASA SP-8005 *Solar Electromagnetic Radiation* (1971), Gilmore ed. *Spacecraft Thermal Control Handbook* vol. 1, 2nd ed., AIAA (2002), and Silverman *Space Environmental Effects on Spacecraft*, NASA CR-4661 (1995).

[19] Standard thermodynamic data for liquid oxygen, liquid methane, and their saturation states at the normal boiling point, including NIST WebBook, NIST REFPROP 10.0 (Lemmon et al., 2018), and NIST-JANAF Thermochemical Tables, 4th ed. (Chase, 1998).

An additional body of work on cryogenic fluid management for orbital applications has been published across the 2010 to 2026 window by groups at NASA Glenn Research Center, NASA Marshall Space Flight Center, NASA Kennedy Space Center, United Launch Alliance, Lockheed Martin Space, Blue Origin, SpaceX, and a number of university groups including Georgia Institute of Technology (Hartwig and colleagues), Purdue University (Vanapalli and colleagues), Case Western Reserve University (Kassemi and colleagues), and ISAE-SUPAERO. The present disclosure extends that body of work by combining six subsystem-level interventions into a single integrated operational architecture specified at Starship scale and ship-to-ship aggregation-campaign scale.

The distinction of the present disclosure over the cited prior art is the integration of all six interventions into a single vehicle and operational architecture processable across a multi-flight aggregation campaign at 1000-ton-class propellant mass. The individual subsystems draw on and extend published and patented prior art. The integrated architecture, and the specific parameter windows and operations sequences that enable integration across a 7-to-60-day aggregation hold with 4-to-more-than-20 tanker flights and 104-meter mated-stack attitude coupling with live mass flow, are not disclosed in the cited art.

§ 4

Summary of the Invention

The present invention provides an integrated orbital propellant aggregation architecture comprising, in coordinated operation, six subsystems deployed across a donor tanker Starship (Component T) and a receiver Starship (Component R):

Component A. Thermal management subsystem

A multi-layer-insulation blanket covering the propellant tank exterior at a residual-heat-flux specification of 1 watt per square meter or better, combined with an active zero-boil-off cryocooler loop extracting residual heat at approximately 34 kilowatts of continuous electrical input during aggregation hold (central design point at 300-K radiator reject).

Component B. Propellant acquisition subsystem

A hybrid passive-plus-active acquisition architecture comprising a surface-tension propellant-management device at the outlet region of each tank, a duty-cycled coast-settling thrust profile at 10^{-5} g during steady aggregation hold, and a transfer-phase settling thrust at 10^{-3} g during active ship-to-ship transfer.

Component C. Slosh mitigation subsystem

An attitude-control and flow-management architecture combining staged flow-rate ramping at transfer start and stop, model-predictive attitude control with explicit augmentation of the fundamental lateral and longitudinal slosh-mode state variables, and on-demand escalation to 10^{-3} g settling when slosh-mode amplitude exceeds a prescribed threshold.

Component D. Mass-gauging subsystem

A multi-sensor fusion architecture comprising fiber-optic distributed temperature sensing along the tank wall, radio-frequency tank-level measurement, and pressure-volume-temperature ullage gauging, combined in a weighted-average estimator with outlier rejection and in-flight cross-calibration, targeting sub-one-percent aggregate mass accuracy at Starship scale.

Component E. Cryogenic androgynous docking subsystem

A metal face seal with cryogenic-resilient plated contact surface, spring-loaded mechanical misalignment-capture hardware, and an autogenous methane purge providing a secondary leak barrier by in-situ condensation on the chilled mating face.

Component F. Mated-stack attitude coupling controller

A model-predictive controller with real-time moment-of-inertia tracking, mass-flow-rate feedforward, and full-state observer including rigid-body modes and slosh modes, commanding the reaction control system of the mated stack in response to center-of-mass drift across live propellant transfer.

The six components, in combination, execute a multi-flight aggregation campaign across a 7-to-60-day low-Earth-orbit hold, with 4 to more than 20 tanker flights depending on the mission class, and with ship-to-ship cryogenic transfer at each tanker arrival. The combined architecture suppresses or manages all six cryogenic-fluid-management challenges concurrently, by six coordinated physical mechanisms: radiative heat interception and active heat pumping (Component A), hybrid capillary-plus-inertial liquid positioning (Component B), active slosh-mode state estimation and flow-regime management (Component C), multi-method sensor cross-validation (Component D), mechanical-and-thermal combined interface management (Component E), and full-dynamics controller-level management of the mated-stack state (Component F).

Quantitative performance target: at the central thermal-flux assumption ($\alpha_s = 0.35$, $\varepsilon_{IR} = 0.12$, orbit-averaged absorbed flux 137 watts per square meter on the tank surface), an MLI-plus-ZBO architecture per Component A drives aggregate propellant loss over a 30-day aggregation hold to below 0.1 percent of inventory, compared with 75 to 100 percent loss on a bare polished-stainless architecture. Combined across all six subsystems, a 15-flight aggregation campaign delivering nominal 1500 metric tons to the receiver closes within approximately 1 percent of the Mars-departure target, with a 16-flight extension available to produce a 7-percent mission margin if the campaign arithmetic requires it. Residual non-cryogenic-fluid-management stack-level mission risks, including deep-space navigation, thermal-protection reusability, and Raptor engine lifetime, are outside the scope of this disclosure and are addressable by separate interventions.

Feature-level novelty claims. The integrated six-subsystem architecture as a whole is the primary subject of this disclosure. Within the combined architecture, three specific feature-level contributions are believed to be disclosed here for the first time and are noted as such for examiner reference:

(i) The multi-sensor fusion architecture of Component D, combining fiber-optic distributed-temperature sensing, radio-frequency tank-level measurement, and pressure-volume-temperature ullage gauging in a weighted-average estimator with outlier rejection and with per-transfer end-to-end in-flight recalibration against donor-delivered mass, is not disclosed in any known prior art, patent or otherwise, at any vehicle scale.

(ii) The use of autogenous methane condensation on a chilled metal face seal to form a solid-methane secondary leak barrier by in-situ condensation *during active transfer* (as distinct from use of methane purge as a pre-mate cleaning or conditioning agent alone), within the cryogenic androgynous docking subsystem (Component E), is believed to be disclosed here for the first time.

(iii) The combined use of real-time moment-of-inertia tracking, mass-flow-rate feedforward, and augmentation of fundamental lateral and longitudinal slosh-mode state variables in the model-predictive-control state vector of a mated-tandem spacecraft pair under continuous inter-vehicle cryogenic fluid transfer, within the attitude coupling controller (Component F), is believed to be disclosed here for the first time.

Each feature-level novelty claim is additive to the overall combined-architecture claim. The overall combined architecture is the primary defensive-publication subject matter under 35 U.S.C. §102.

§ 5

Detailed Description of the Preferred Embodiment

The preferred embodiment is described below in seven subsections. Subsection 5.1 specifies the thermal management subsystem (Component A). Subsection 5.2 specifies the propellant acquisition subsystem (Component B). Subsection 5.3 specifies the slosh mitigation subsystem (Component C). Subsection 5.4 specifies the mass-gauging subsystem (Component D). Subsection 5.5 specifies the cryogenic androgynous docking subsystem (Component E). Subsection 5.6 specifies the mated-stack attitude coupling controller (Component F). Subsection 5.7 specifies the integration architecture, the operations sequence of a single tanker transfer, and the campaign-level aggregation sequence. Numbered reference elements consistent with the figures in Section 10 are used throughout the description for unambiguous mapping between text and drawings.

REFERENCE NUMERAL KEY (USED THROUGHOUT §5 AND FIGURES)

10	Donor tanker Starship
20	Receiver Starship
30	Mated-stack mechanical interface
40	Thermal management subsystem (Component A)
40a	Multi-layer-insulation blanket (external tank surface)
40b	Active cryocooler cold head (interior tank wall)
40c	Cryocooler waste-heat radiator
40d	Optional vapor-cooled shield (intermediate layer)
50	Propellant acquisition subsystem (Component B)
50a	Outlet-region propellant management device (tank interior)
50b	Coast-settling thrust generator (reaction-control cluster, duty-cycled)
50c	Transfer-settling thrust generator (continuous, 10^{-3} g regime)
60	Slosh mitigation subsystem (Component C)
60a	Staged-flow transfer valve
60b	Slosh-state estimator (flight software)
60c	Slosh-mode fill-interface sensor array
70	Mass-gauging subsystem (Component D)
70a	Distributed fiber-optic temperature sensor (tank wall)
70b	Radio-frequency tank-level antenna
70c	Pressure-volume-temperature ullage sensor
70d	Fusion estimator (flight software)
80	Cryogenic androgynous docking subsystem (Component E)
80a	Metal face seal with cryogenic-resilient plating
80b	Autogenous methane purge port
80c	Spring-loaded mechanical-capture latch array
80d	Mechanical-alignment feature (cone-and-socket or petaloid)

90	Mated-stack attitude coupling controller (Component F)
90a	Model-predictive-control solver (flight software)
90b	Reaction-control thruster cluster (mated-stack authority)
90c	Moment-of-inertia tracker (flight software)
100	Donor LOX tank
110	Donor methane tank
120	Receiver LOX tank
130	Receiver methane tank
140	Liquid-transfer umbilical (LOX line and CH_4 line)
150	Vapor-return umbilical
160	Autogenous pressurization manifold
170	Mated-stack common structural axis

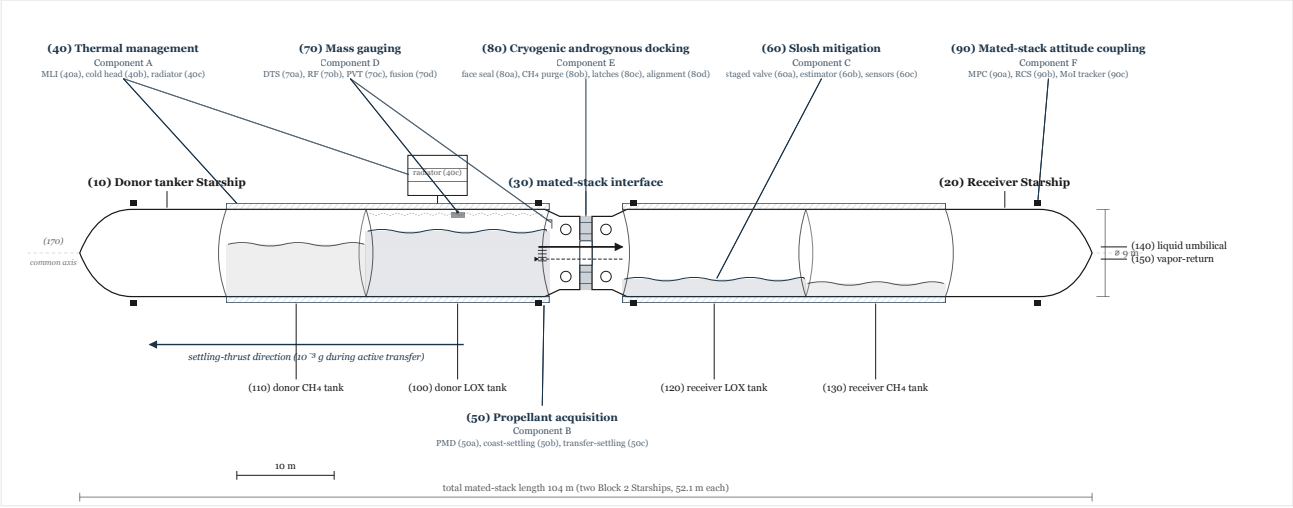

Figure 1. Mated-stack overall schematic. Two Block 2 Starships (approximately 52.1 m each) mate tail-to-tail along the mated-stack common structural axis (170) at a total mated-stack length of approximately 104 m. The donor tanker (10) is at left and the receiver Starship (20) is at right, joined through the mated-stack mechanical interface (30). Donor LOX tank (100), donor methane tank (110), receiver LOX tank (120), and receiver methane tank (130) are labeled; the liquid-transfer umbilical (140) and vapor-return umbilical (150) pass through the central bore of the docking interface. Arrows indicate propellant flow direction and settling-thrust direction during active transfer.

§ 5.1 Thermal management subsystem (40)

The thermal management subsystem (40) controls radiative and conducted heat load on the propellant tanks of both the donor (10) and the receiver (20) throughout the aggregation-hold interval. The subsystem combines a passive multi-layer-insulation blanket (40a) applied to the exterior tank surface with an active cryocooler loop (40b, 40c) for zero-boil-off service.

Composition

The MLI blanket (40a) comprises 40 to 80 layers (preferred 60 layers) of double-aluminized Mylar film or double-aluminized Kapton film (for high-temperature operation near thrust-structure heat-soak zones), separated by Dacron netting spacers of mesh opening 1 to 3 millimeters. Outer facing layer is aluminized Kapton for atomic-oxygen resistance at LEO altitudes; inner facing layer is aluminized Mylar. Installed areal mass is 0.5 to 0.8 kilogram per square meter, with 0.6 kilogram per square meter as the preferred value.

Coverage

MLI blanket (40a) covers the exterior of the LOX tank (100, 120), the exterior of the methane tank (110, 130), and the common intertank dome. Tank penetrations (feed lines, instrumentation ports, vent lines) are individually insulated with matching-performance MLI sleeves. Installation seams are laid with 50-millimeter overlap and taped with aluminized-Kapton pressure-sensitive tape.

Residual heat flux specification

The installed MLI blanket is specified to achieve a residual heat flux of 1 watt per square meter or better, measured on a representative tank-surface installation in ground thermal-vacuum test against a boundary-temperature differential of 300 kelvin to 90 kelvin. Field-installation performance of 1.5 to 2.5 watts per square meter is acceptable as a derated specification and is accommodated by Component A sizing margin.

Active cryocooler cold head (40b)

Each propellant tank (LOX and methane, both donor and receiver) is equipped with an internal cold head mounted on the tank dome that removes residual heat from the liquid propellant by direct contact with the tank wall or by a dedicated internal heat exchanger. The cold-head operating temperature is held within 2 to 5 kelvin below the propellant saturation temperature at the ullage pressure. For LOX at 1 atmosphere ullage (saturation 90.2 K), the cold-head temperature is in the range 85 to 88 K. For methane at 1 atmosphere ullage (saturation 111.7 K), the cold-head temperature is in the range 107 to 110 K.

Cryocooler cycle and sizing

The cryocooler is a reverse-Brayton cycle or single-stage Stirling cycle sized to reject 100 to 200 watts thermal per cold head at the operating temperature. Two cold heads per tank (one on each dome) for redundancy and uniform heat extraction. For a Starship methalox tank pair with 130 kilowatts absorbed heat at bare-stainless thermal conditions and 950 m² external surface area, the MLI reduces the heat reaching the propellant to approximately 0.95 kilowatts. Active ZBO extracts this heat at electrical-to-thermal-pumping efficiency set by the Carnot limit modified by a real-cryocooler fraction of approximately 5 to 10 percent at LOX temperatures and 6 to 12 percent at methane temperatures. The resulting electrical input at 300-kelvin radiator reject is approximately 25 kilowatts at the LOX side (0.53 kW at 5% of 0.43 Carnot COP) and approximately 9 kilowatts at the methane side (0.42 kW at 8% of 0.59 Carnot COP), combining to approximately 34 kilowatts continuous draw. At a radiator (40c) reject temperature of 250 kelvin (shadowed radiator), this falls to approximately 25 kilowatts.

Waste-heat radiator (40c)

The cryocooler warm end rejects waste heat to a deployable or fixed radiator located on the shadow side of the vehicle during aggregation hold. Preferred radiator is a double-sided aluminum-honeycomb panel with heat-pipe internal distribution and Z93-white optical coating (solar absorptance 0.15, infrared emittance 0.85). Radiator sizing delivers 50 to 70 kilowatts thermal at 250 to 300 kelvin reject temperature, sized for worst-case solar orientation with margin. Total radiator area approximately 200 to 300 square meters. Deployable radiator architectures are the preferred embodiment for stowage during launch and ascent.

Optional vapor-cooled shield (40d)

In a further embodiment, cold vented vapor from the primary tank is routed through a secondary shield interposed between the MLI blanket (40a) and the primary tank wall. The vapor-cooled shield intercepts heat before it reaches the propellant and reduces the residual heat flux by 30 to 50 percent, with corresponding reduction in cryocooler electrical load. This embodiment is preferred for aggregation campaigns exceeding 30 days or for vehicles with reduced solar-array power margin.

Power source

Electrical input to the cryocooler is supplied by the donor vehicle's solar array and battery system, sized to cover continuous cryocooler load plus bus services. Estimated array power requirement on the aggregation-hold receiver: 55 to 75 kilowatts end-of-life, depending on cryocooler regime and radiator reject temperature. This is within the envelope of deployable gallium-arsenide or triple-junction solar arrays at 300 watts per square meter array-level, requiring approximately 180 to 250 square meters of solar-array area.

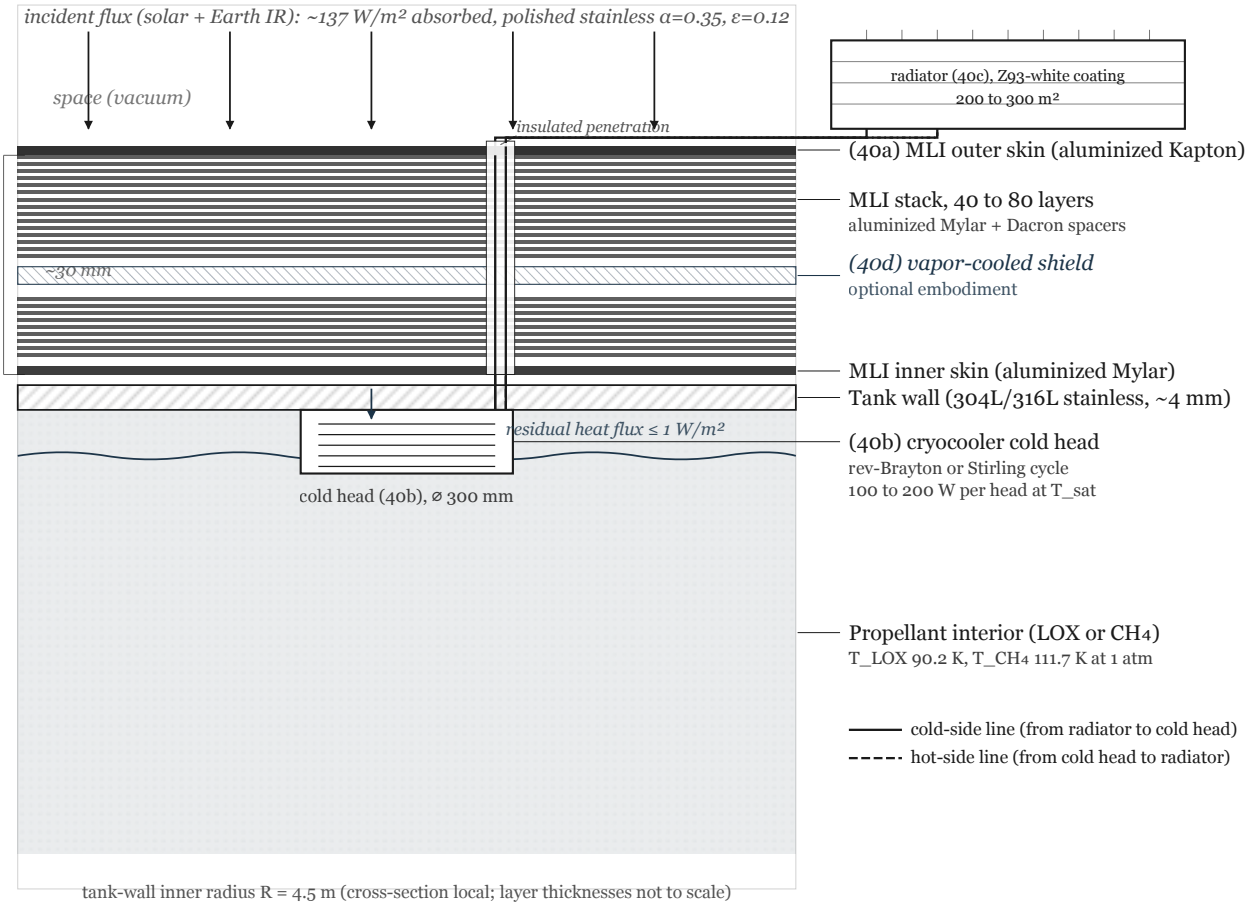

Figure 2. Thermal management subsystem cross-section at representative tank mid-height. From exterior to interior: incident solar and Earth-IR flux (approximately 137 W/m² absorbed, polished stainless α=0.35, ε=0.12); multi-layer-insulation blanket (40a), 40 to 80 layers of aluminized Mylar with Dacron spacers, residual heat flux 1 W/m² or better; optional vapor-cooled shield (40d) interposed within the stack; stainless-steel tank wall; propellant interior (LOX 90.2 K or methane 111.7 K at 1 atm). An internal cryocooler cold head (40b), 300 mm diameter, is mounted on the tank interior; a heat-pipe loop routes hot fluid through an insulated MLI penetration to a deployable waste-heat radiator (40c) with Z93-white optical coating at 200 to 300 m² total area. Layer thicknesses not to scale.

§ 5.2 Propellant acquisition subsystem (50)

The propellant acquisition subsystem (50) positions liquid cryogen at the tank outlet in the zero-gravity environment of low Earth orbit, ensuring vapor-free delivery of liquid into the transfer line during active ship-to-ship transfer. The subsystem combines a surface-tension propellant management device at the outlet region (50a) with duty-cycled coast-settling thrust (50b) and continuous transfer-settling thrust (50c).

Outlet-region PMD (50a)

Each tank outlet is preceded by a passive propellant management device comprising a vane-and-sponge structure sized to hold 100 to 500 liters of propellant against modest residual-g forces (up to 10^{-4} g) by surface-tension channeling. The PMD comprises radially oriented vanes of thickness 0.2 to 0.5 millimeter, vane spacing 5 to 15 millimeters, and total vane height 100 to 300 millimeters. Vane material is 304L or 316L stainless steel matching the tank material. A sponge region of 50 to 100 millimeter thickness composed of perforated-plate stacks or open-cell metal foam with pore size 0.5 to 2 millimeter is mounted between the vanes and the outlet pipe to hold the immediate-outlet-volume liquid against the outlet face.

PMD function

The PMD (50a) does not attempt to hold the bulk propellant mass. Its function is limited to two narrow roles: outlet-region liquid retention at the start of a transfer (during the first 1 to 5 seconds of flow before bulk-propellant arrival at the outlet under settling thrust); and start-stop transient management during pulsed flow (keeping the outlet pipe wet across brief flow interruptions). The bulk propellant mass is positioned by settling thrust (50b, 50c).

Coast-settling thrust generator (50b)

During the aggregation-hold interval between active transfers, a duty-cycled settling thrust of 10^{-5} g is applied to the receiver for 5 to 15 minutes once per orbit (orbital period approximately 90 minutes at 400 kilometers altitude), repositioning the bulk propellant mass against the outlet-end tank dome. Preferred duty cycle is 10 minutes of settling per 90-minute orbit, equivalent to an 11 percent duty cycle. The settling thrust is delivered by the receiver vehicle's reaction-control-system thrusters firing in the anti-velocity direction. Receiver mass grows stepwise across the campaign from approximately 160 metric tons (pre-transfer 1) to approximately 1660 metric tons (post-transfer 15), so required thrust at 10^{-5} g ranges from approximately 16 to 163 newtons. At autogenous warm-gas methalox specific impulse (Isp approximately 300 seconds), the coast-settling reaction mass across a 30-day campaign integrates stepwise to approximately 8.3 metric tons at the 11 percent duty cycle (worked in §7.3).

Transfer-settling thrust generator (50c)

During active ship-to-ship transfer, a continuous settling thrust of 10^{-3} g is applied for the duration of the transfer (typically 20 to 40 minutes per tanker-to-receiver transfer). Combined mated-stack mass varies across a 15-flight aggregation campaign from approximately 430 metric tons (transfer 1, receiver near-empty) to approximately 1830 metric tons (transfer 15, receiver near-full), so required thrust at 10^{-3} g ranges from approximately 4 to 18 kilonewtons. This is delivered by a throttleable cluster of mid-thrust engines firing along the mated-stack common axis in the anti-velocity direction. Preferred implementation is two 10-kilonewton-class methalox thrusters per vehicle with a 3-to-1 throttle range, operating at autogenous warm-gas methalox specific impulse (Isp approximately 300 seconds on scavenged CH4/O2 per the ULA Integrated Vehicle Fluids architecture, U.S. Patent 10,717,550). The per-transfer reaction-mass cost ranges from approximately 2.6 metric tons (transfer 1) to approximately 11 metric tons (transfer 15). Total transfer-settling propellant across a 15-flight campaign is approximately 102 metric tons, booked explicitly in §7.3.

Liquid-transfer umbilical (140)

Propellant transfer between donor and receiver tanks is effected by a pair of cryogenic liquid-transfer lines (one for LOX, one for methane) routed through the mated-stack interface (30) per §5.5. Transfer-line internal diameter is 150 to 250 millimeters per line, sized for a volumetric flow rate of 500 to 1500 liters per second at nominal transfer-line pressure of 6 to 10 bar absolute. Transfer-line material is 304L or 316L austenitic stainless steel, vacuum-jacketed with MLI insulation along the full length exposed outside the mated-stack interface.

Vapor-return umbilical (150)

A dedicated vapor-return line between receiver ullage and donor ullage equalizes tank pressures during transfer, preventing donor tank underpressure and receiver overpressure. Vapor-return line internal diameter is 100 to 150 millimeters, routed alongside the liquid-transfer lines through the mated-stack interface. In a preferred embodiment, the vapor-return line is used for no-vent-fill operation at the receiver, in which ullage gas is compressed by the incoming liquid and routed back to the donor (no venting to space), eliminating vent-loss propellant mass across the aggregation campaign.

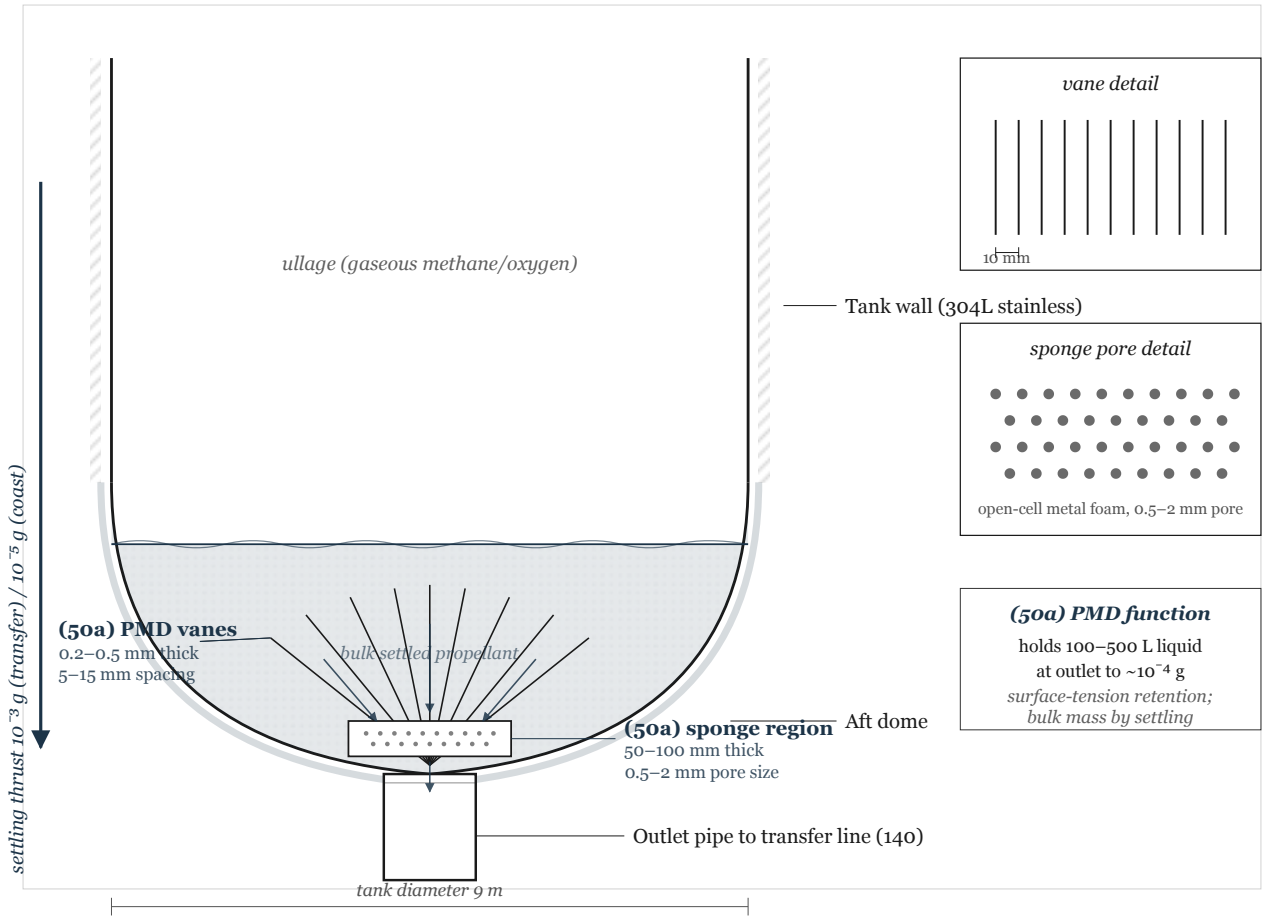

Figure 3. Propellant acquisition subsystem detail at the tank outlet. Bulk propellant has settled against the aft dome under 10^{-3} g (active transfer) or 10^{-5} g (coast). The outlet-region PMD (50a) sits above the outlet pipe and comprises radial vanes (0.2 to 0.5 mm thick, 5 to 15 mm spacing) and a perforated-plate sponge (50 to 100 mm thickness, 0.5 to 2 mm pore size). The PMD holds 100 to 500 liters of propellant at the outlet against residual-g up to 10^{-4} g by surface-tension channeling; bulk propellant mass is positioned by settling thrust. Tank diameter 9 m.

§ 5.3 Slosh mitigation subsystem (60)

The slosh mitigation subsystem (60) manages the coupling between flow-rate transients, imposed accelerations, and natural slosh modes of the liquid propellant volume across the aggregation hold and across individual transfer events. The subsystem combines staged flow-rate management (60a), active slosh-mode state estimation (60b), and on-demand transition between coast-gravity and settling-gravity regimes.

Staged-flow transfer valve (60a)

The liquid-transfer umbilical (140) is regulated by a variable-area flow control valve that ramps flow rate at transfer start and stop across a configurable ramp duration. Preferred ramp is linear flow increase from zero to full nominal rate across 60 to 180 seconds at transfer start, and linear flow decrease across 60 to 180 seconds at transfer stop. The ramp rate is set below the fundamental slosh-mode bandwidth to avoid resonant excitation. At the preferred 120-second ramp, the ramp rate is approximately 5 to 10 liters per second per second, below the 10^{-2} hertz slosh-mode bandwidth at coast-gravity.

Slosh-state estimator (60b)

An onboard flight-software module estimates the instantaneous slosh state (fundamental lateral mode amplitude and phase; fundamental longitudinal mode amplitude and phase; second-harmonic lateral mode amplitude and phase) in each tank. The estimator is a Kalman-filter implementation with state vector of dimension 12 to 24 per tank (four states per mode × three to six modes tracked), updated at 10 hertz. Measurements fused by the estimator include slosh-mode fill-interface sensor readings (60c), tank-wall strain-gauge readings, and attitude-sensor readings from the vehicle's inertial measurement units. Estimator initialization occurs during a dedicated 5-minute settling-burn calibration sequence at the start of each aggregation campaign.

Slosh-mode fill-interface sensor array (60c)

Inside each tank, a linear array of 8 to 16 capacitance or ultrasonic liquid-vapor interface sensors is mounted along the tank vertical axis (under settling-thrust reference frame) at axial intervals of 2 to 4 meters. Each sensor registers presence or absence of liquid at its location. Time history of interface crossings across the array provides direct measurement of the lateral slosh-mode amplitude, with signal-to-noise ratio adequate to distinguish amplitude variations of 50 millimeter or larger.

Coast-to-settling transition logic

A flight-software decision logic monitors slosh-state amplitude in real time. When the estimated fundamental-mode amplitude in any tank exceeds a prescribed threshold (preferred 2 meters peak-to-peak in the lateral mode), the system escalates from 10^{-5} g coast settling to 10^{-3} g firm settling for a dwell interval of 5 to 30 minutes, or until the estimated amplitude returns below a hysteresis-offset re-entry threshold (preferred 0.5 meters). The transition consumes approximately 320 kilograms per minute of reaction mass at autogenous warm-gas methalox Isp (per Component B propulsion commitment), booked against the campaign settling budget.

§ 5.4 Mass-gauging subsystem (70)

The mass-gauging subsystem (70) measures the instantaneous mass of liquid propellant in each tank of both donor and receiver vehicles across the aggregation campaign to better than 1 percent aggregate accuracy. The subsystem combines distributed fiber-optic temperature sensing (70a), radio-frequency tank-level measurement (70b), and pressure-volume-temperature ullage gauging (70c), with weighted-average fusion logic (70d).

Distributed fiber-optic temperature sensor (70a)

A single-mode optical fiber of length 150 to 300 meters per tank is routed along the tank wall interior in a helical pattern with pitch spacing 200 to 500 millimeters. The fiber is interrogated by a ground-qualified distributed-temperature-sensing instrument (Raman or Brillouin backscatter) at the vehicle-side bulkhead, producing a temperature reading at 0.5 to 1 meter spatial resolution with temperature accuracy of 0.5 to 1 kelvin. The liquid-vapor interface is inferred from the temperature transition signature. Mass is inferred from the liquid-fraction cross-section of the tank at each sensor axial position, integrated across the tank length. Nominal accuracy on ground test: 0.5 to 2 percent of total tank volume.

Radio-frequency tank-level sensor (70b)

An RF antenna array mounted at the tank dome transmits a chirped waveform (frequency 2 to 8 gigahertz) and receives reflections from the liquid-vapor interface. Time-domain and frequency-domain analysis of the reflection spectrum yields a tank-level measurement with accuracy 1 to 3 percent of tank volume. The RF method is sensitive to internal tank geometry and to propellant dielectric properties but is insensitive to temperature gradients that degrade DTS accuracy, providing an independent and uncorrelated cross-check.

Pressure-volume-temperature ullage sensor (70c)

Tank ullage pressure, ullage temperature, and known-geometry ullage volume combine through the ideal-gas law (corrected for ullage composition) to yield a mass estimate by subtraction from total tank volume. PVT accuracy in nominal conditions is 3 to 5 percent. The PVT subsystem is used primarily as a composition-integrity sensor: a divergence between PVT-inferred mass and DTS-or-RF-inferred mass indicates ullage composition drift (water vapor, nitrogen contamination, methane-oxygen cross-diffusion), flagging the nominal propellant-mass estimate for correction.

Fusion estimator (70d)

A flight-software fusion module combines DTS, RF, and PVT measurements in a weighted-average estimator with inverse-variance weighting per sensor and outlier-rejection logic. When the three methods agree within their stated uncertainty envelopes, the fused estimate has variance below any individual method by a factor of approximately √3. When one method flags an outlier (typically PVT flagging an ullage composition drift), the estimator downweights the flagged method and flags the measurement for ground review. Target aggregate accuracy: 0.3 to 1 percent of total tank mass at Starship scale.

In-flight recalibration

At each tanker transfer, the known-mass increment (mass delivered by the departing tanker, reported by its own mass-gauging subsystem) provides an end-to-end cross-calibration against the receiver's fusion-estimator readings before and after transfer. Any systematic bias is recorded and tracked across the aggregation campaign. The calibration improves the sub-one-percent accuracy target by providing a continuous ground-truth reference against the sensor-fusion estimate.

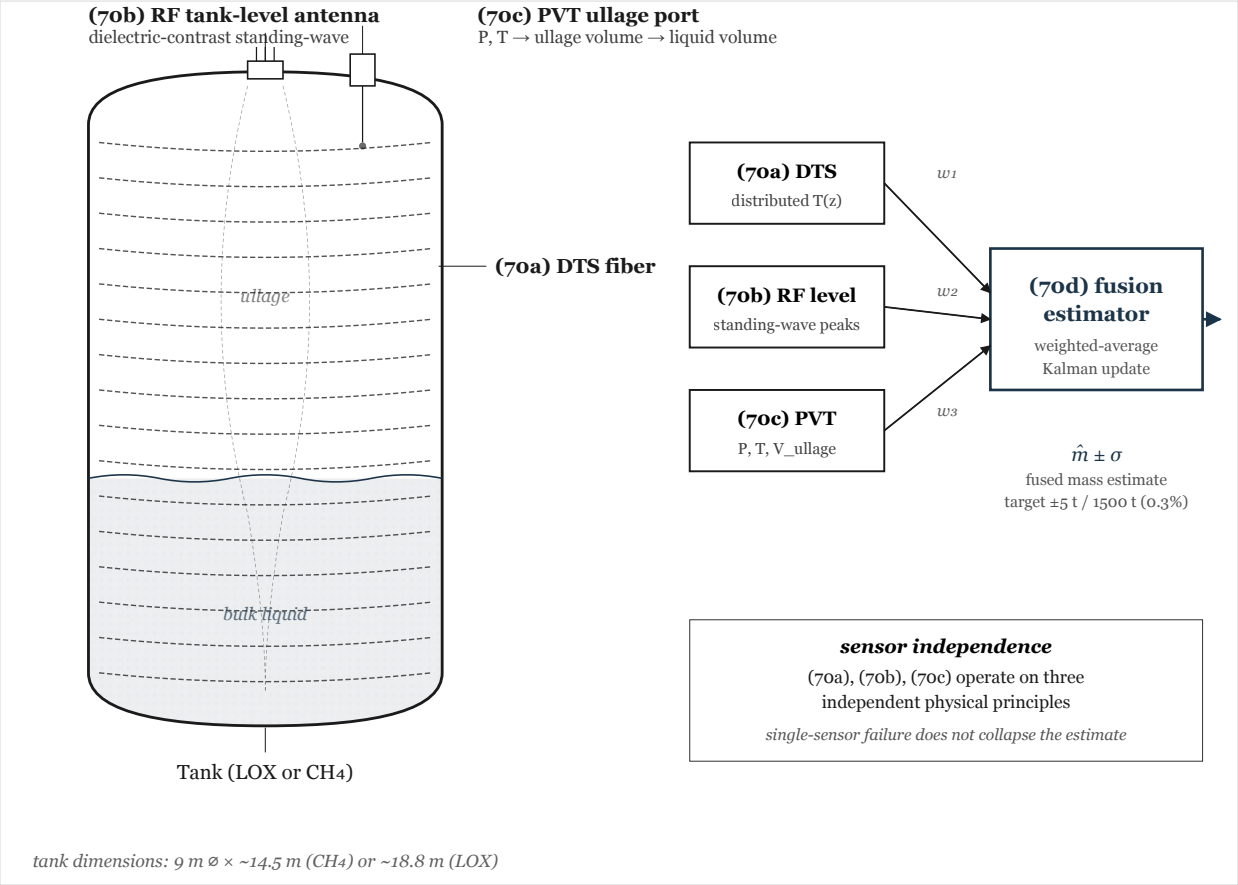

Figure 4. Mass-gauging subsystem sensor layout and fusion-estimator block diagram. Left: a transparent-tank schematic showing the distributed fiber-optic temperature sensor (70a) in helical pattern along the tank wall interior, the RF tank-level antenna (70b) mounted at the tank dome, and the PVT ullage-sensor port (70c). Right: block diagram of the fusion estimator (70d) combining the three inputs through inverse-variance weighted averaging with outlier rejection, producing a fused mass estimate to the 0.3-to-1-percent aggregate accuracy target.

§ 5.5 Cryogenic androgynous docking subsystem (80)

The cryogenic androgynous docking subsystem (80) effects ship-to-ship mechanical mating at the mated-stack interface (30) and cryogenic-fluid transfer across that interface throughout the aggregation campaign. The subsystem comprises a metal face seal (80a), an autogenous methane purge (80b), spring-loaded mechanical-capture latches (80c), and a mechanical-alignment feature (80d).

Metal face seal (80a)

The liquid-propellant transfer line passes through the mated-stack interface on a metal face seal comprising two planar or near-planar metal surfaces in sealed contact under axial compression. Preferred seal geometry is a flat stainless-steel face on the receiver side mating against a flat plated stainless-steel face on the donor side, with seal diameter matched to the transfer-line internal diameter (150 to 250 millimeters). Preferred plating is electroless nickel of 5 to 20 micrometer thickness, or sputter-deposited NiAl or TiN of 1 to 5 micrometer thickness. Plating selection provides a hard, cryogenic-resilient contact surface with low-friction repeated-mate behavior. Seal compression force is delivered by the mechanical-capture latch array (80c) at approximately 20 to 50 kilonewtons axial force across the seal face.

Seal performance and cycle life

The metal face seal achieves a leak rate below 10^{-6} mbar·L/s at 90 kelvin operating temperature, measured in ground cryogenic-seal-test fixtures. Mate-demate cycle life without detectable seal degradation is approximately 1000 to 5000 cycles, based on wear-rate scaling from cryogenic-valve-seat testing. Per-tanker mate-demate count of 1 combined with a 1000-cycle seal lifetime supports a Mars-campaign fleet-scale mate inventory of 1000 tankers. Scheduled seal-face re-plating is supported at 500-cycle intervals without disassembly of the vehicle.

Autogenous methane purge (80b)

Prior to primary mate, both seal faces are conditioned to 90 kelvin equilibrium by 60 to 120 seconds of purge with gaseous methane from the donor methane tank ullage, routed through a dedicated purge port (80b) in each seal face. The methane condenses on the chilled seal surfaces during conditioning, forming a solid methane coating of thickness 0.01 to 0.1 millimeter. The solid methane layer serves two functions: (a) as a primary-seal conditioning agent that cleans and wets the seal face before primary contact, reducing debris-induced leakage; and (b) as an in-situ secondary leak barrier during transfer, in which any micro-leak in the primary metal seal is locally sealed by continued re-condensation of methane vapor on the cold surface throughout the transfer interval. The purge pressure at the seal face is monitored via an embedded pressure port to confirm condensation coverage before committing to mate. Helium purge is available as a fallback at 1 to 3 kilograms per mate event, in the event that autogenous methane purge underperforms in flight.

The use of continuous autogenous methane condensation on the cryogenic metal face seal as an active secondary leak barrier during active transfer, distinct from methane purge used only as a pre-mate conditioning agent, is believed to be disclosed here for the first time. Prior-art disclosures of methane purge in cryogenic fittings (industrial LNG transfer, NASA KSC-TOPS-63 low-separation-force quick disconnect) treat the purge as a pre-mate cleaning step and terminate the purge prior to flow establishment. The present disclosure maintains a continuous low-flow methane condensation circuit

throughout the transfer interval, using the donor's ullage pressure to replenish vapor as it condenses on the cold seal face, such that any micro-leak in the primary metal seal is locally re-sealed on a continuous basis across the full transfer interval.

Spring-loaded mechanical-capture latch array (80c)

A ring of 6 to 12 spring-loaded latches distributed around the seal circumference engages mating features on the receiver face during final approach, providing axial compression and bending-moment reaction at the interface. Each latch delivers 2 to 5 kilonewtons of axial capture force and 5 to 15 kilonewtons of peak shock-load tolerance. Latch material is titanium Ti-6Al-4V or Inconel 718 for cryogenic-compatible fracture toughness. Release mechanism is motor-driven retraction of the latch hook, executed on command for demate.

Mechanical-alignment feature (80d)

A cone-and-socket or petaloid alignment feature at the seal circumference provides passive axial and rotational alignment during final approach, tolerant to ±5 centimeter lateral misalignment and ±2 degree angular misalignment at the initiation of final-approach closure. Alignment-feature material is 17-4PH stainless steel or Inconel 625 for cryogenic compatibility combined with wear resistance.

Contamination management

Between transfers, the seal faces are covered by a retractable cover plate that prevents ice formation and debris accumulation during aggregation-hold intervals. The cover plates are retracted on command prior to mate and re-deployed on demate. In a further embodiment, a mechanical wiper sweeps the seal face immediately before primary mate, removing any accumulated contamination.

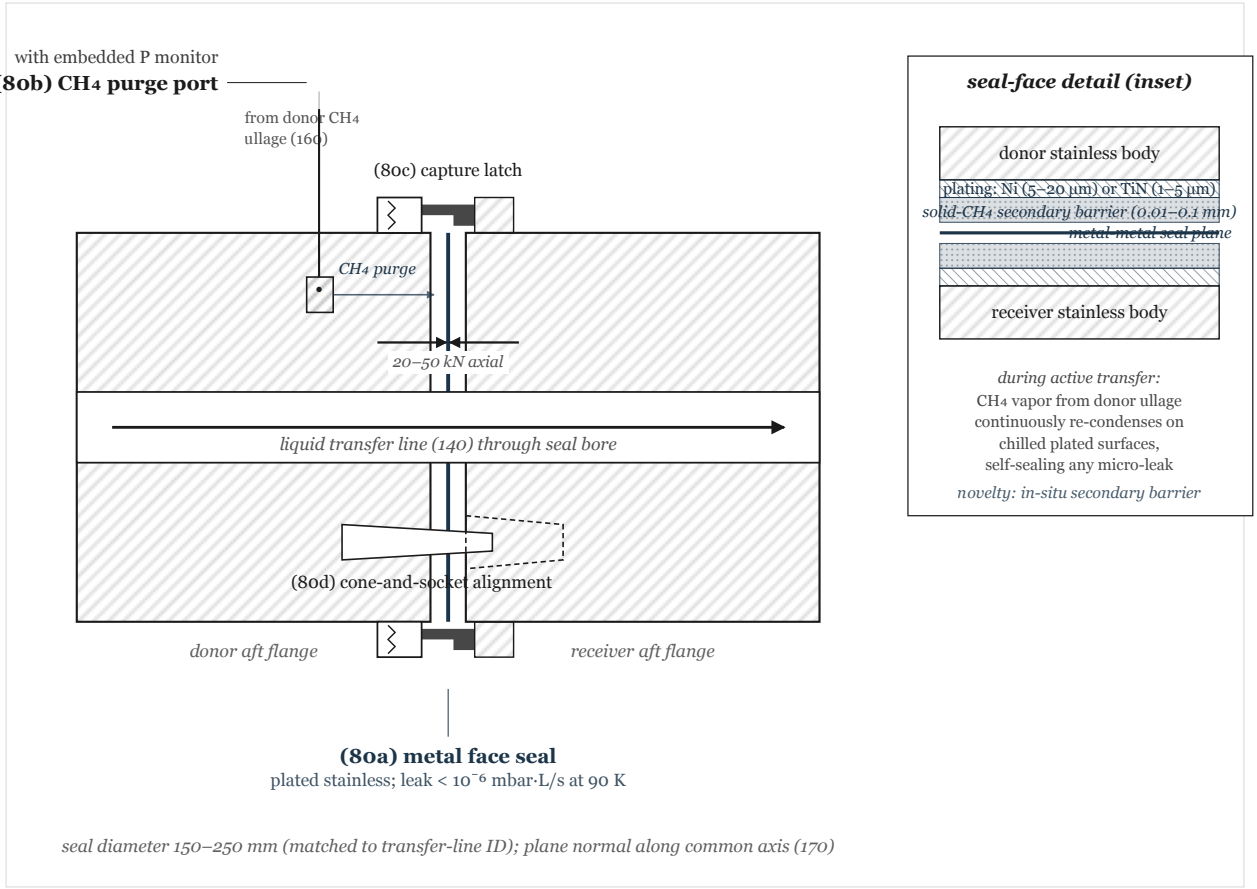

Figure 5. Cryogenic androgynous docking interface cross-section. Donor and receiver flanges (hatched) mate symmetrically against a planar metal face seal (80a), plated with electroless Ni (5 to 20 µm) or sputter TiN (1 to 5 µm), achieving leak rate below 10^{-6} mbar·L/s at 90 K. Spring-loaded mechanical-capture latches (80c) deliver 20 to 50 kN axial compression. A cone-and-socket alignment feature (80d) provides passive ±5 cm / ±2° tolerance. An autogenous methane purge port (80b) with embedded pressure monitor delivers gaseous methane from the donor ullage (160) to both seal faces for pre-mate conditioning and for continuous in-situ secondary-barrier formation during active transfer. The inset shows the seal-face plating structure and the solid-CH_4 secondary barrier (0.01 to 0.1 mm) that forms and continuously re-condenses on the chilled plated surfaces during transfer.

§ 5.6 Mated-stack attitude coupling controller (90)

The mated-stack attitude coupling controller (90) manages the attitude and center-of-mass dynamics of the mated-tandem vehicle pair across live propellant transfer. The controller comprises a model-predictive-control solver (90a) operating on a full-dynamics model of the mated stack, commanding reaction-control-system authority (90b) with reference to a moment-of-inertia tracker (90c).

Model-predictive-control solver (90a)

A flight-software module formulates the combined-stack attitude-control problem as a quadratic program with horizon 30 to 60 seconds and update rate 10 hertz. The dynamics model includes six rigid-body modes (three translational, three rotational), 6 to 12 slosh modes per tank (fundamental plus harmonics of lateral and longitudinal modes), and a continuously updated mass-inertia parameter set provided by the moment-of-inertia tracker (90c). Control variables are the individual thrust commands for each reaction-control cluster on both donor and receiver. Constraints include thruster saturation limits, pointing-envelope margins, and slosh-amplitude hysteresis bounds.

Reaction-control thruster cluster (90b)

The mated stack employs reaction-control thrusters on both donor and receiver vehicles, coordinated through the MPC solver. Per-vehicle RCS authority is approximately 10 to 50 kilonewton-meter at the vehicle level, combining to 20 to 100 kilonewton-meter net torque on the mated stack. In a preferred embodiment, additional RCS clusters are mounted near the mated-stack interface (30) to deliver direct 100 to 500 kilonewton-meter torque authority at the interface, reducing the lever-arm penalty of vehicle-extremity thruster placement.

Moment-of-inertia tracker (90c)

A flight-software module computes the instantaneous moment-of-inertia tensor of the mated stack at 1-hertz update rate. Inputs include donor and receiver tank mass readings from the mass-gauging subsystem (70), tank-internal mass distribution from settled-gravity equilibrium under the current settling thrust, and the known geometry of the mated-stack common structural axis (170). The tracker feeds the MPC solver (90a) at a rate consistent with the control-loop bandwidth, permitting the controller to respond to changing dynamics across live transfer.

Mass-flow feedforward

The MPC solver (90a) receives a feedforward signal from the liquid-transfer flow rate reported by the transfer-control system (part of Component B), permitting the controller to anticipate center-of-mass drift at the rate of mass transfer. At the per-transfer combined flow rate of approximately 55 kilograms per second (100-tonne delivery across a 30-minute transfer interval, split approximately 43 kg/s LOX and 12 kg/s methane), the feedforward signal reduces peak attitude error by approximately a factor of two compared with a feedback-only control loop.

Coast-to-settling transition coordination

The MPC controller (90a) coordinates with the slosh-state estimator (60b) to command transition between coast-gravity (10^{-5} g) and settling-gravity (10^{-3} g) regimes based on slosh-mode amplitude and attitude-error tolerance. The transition is executed with continuity of the control-law state across the regime boundary.

The combined use of real-time moment-of-inertia tracking (90c), mass-flow-rate feedforward from the transfer-control system, and augmentation of fundamental lateral and longitudinal slosh-mode state variables in the MPC state vector for a mated-tandem spacecraft pair under continuous inter-vehicle cryogenic fluid transfer is believed to be disclosed here for the first time. Prior-art single-spacecraft MPC implementations (for example Weiss, Zlotnik, Di Cairano, MERL, U.S. Patent 10,967,991 B2) do not include mated-tandem vehicle dynamics, do not include real-time moment-of-inertia tracking under continuous inter-vehicle mass transfer at the rate and scale specified here, and do not include slosh-mode state augmentation at low-frequency coast-gravity fundamental periods. The present disclosure's combined treatment of these three elements in a single MPC formulation is the feature-level novelty claim for Component F.

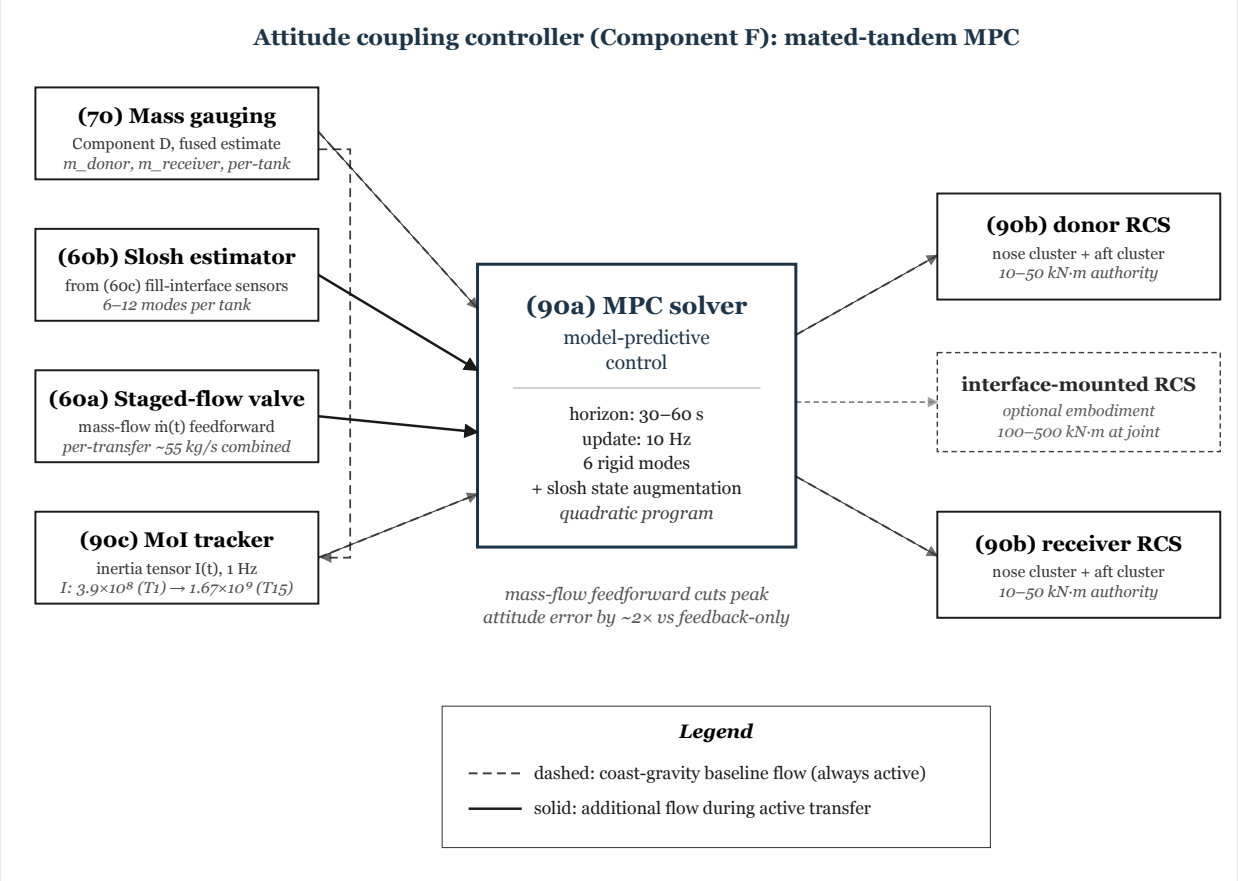

Figure 6. Mated-stack control architecture block diagram. The MPC solver (90a) runs as a quadratic program at 10 Hz with a 30-to-60-second horizon, receiving dashed (coast-baseline) inputs from the mass-gauging subsystem (70) and the moment-of-inertia tracker (90c), and solid (transfer-only) inputs from the slosh-state estimator (60b) and the staged-flow valve (60a) mass-flow feedforward. Outputs command the reaction-control thruster clusters (90b) on both donor and receiver; an optional interface-mounted RCS cluster provides augmented 100-to-500 kN·m torque authority directly at the mated-stack joint. The mass-flow feedforward reduces peak attitude error by approximately 2× relative to feedback-only control.

§ 5.7 Integration architecture and operations sequence

The six subsystems are integrated across the donor and receiver vehicles and operated according to a defined sequence at both the single-transfer scale and the campaign scale.

Single-transfer operations sequence. For each tanker arrival at the receiver:

1. **Approach phase.** Donor tanker performs autonomous rendezvous to within 50 meters of the receiver. Both vehicles enter matched coast-gravity attitude and initiate pre-mate conditioning of docking subsystems (80). Duration: approximately 4 to 8 hours from launch.

2. **Pre-mate conditioning.** Retractable cover plates on seal faces are withdrawn. Autogenous methane purge (80b) is initiated on both seal faces, conditioning them to 90 kelvin equilibrium across a 60 to 120 second interval. Purge-face pressure is monitored to confirm condensation coverage.

3. **Final approach and mate.** Donor tanker executes final-approach closure to the receiver, guided by optical and RF proximity sensors. Mechanical alignment feature (80d) engages at approximately 10 centimeter final-approach distance, providing passive axial alignment. Spring-loaded capture latches (80c) engage at contact, delivering axial compression across the metal face seal (80a). Duration: approximately 2 to 5 minutes.

4. **Transfer-settling thrust ramp.** Transfer-settling thrust generator (50c) initiates 10^{-3} g continuous settling, applied along the mated-stack common axis (170). Slosh-state estimator (60b) is activated in each tank. Attitude controller (90a) transitions to transfer-regime tuning.

5. **Staged flow ramp-up.** Staged-flow transfer valve (60a) ramps liquid flow from zero to nominal transfer rate across 60 to 180 seconds, within the sub-slosh-bandwidth envelope.

6. **Steady transfer.** Liquid propellant flows from donor tanks (100, 110) through liquid-transfer umbilical (140) to receiver tanks (120, 130) at nominal rate 500 to 1500 liters per second per line. Vapor-return umbilical (150) equalizes pressure. Mass-gauging fusion (70d) tracks both vehicles' propellant mass in real time. MPC attitude controller (90a) compensates center-of-mass drift. Duration: approximately 20 to 40 minutes.

7. **Staged flow ramp-down.** Transfer-valve (60a) ramps flow from nominal rate to zero across 60 to 180 seconds.

8. **Transfer-settling thrust termination.** Settling thrust (50c) is terminated. Mated stack returns to coast-gravity attitude.

9. **Post-transfer mass reconciliation.** Donor-and-receiver mass-gauging readings are compared. The difference between donor-reported mass delivered and receiver-reported mass received is recorded as the per-transfer closure metric, used for in-flight recalibration of the fusion estimator (70d) per §5.4.

10. **Demate and separation.** Autogenous methane purge pressure is released. Mechanical-capture latches (80c) retract on command. Donor separates from receiver under residual-g with small anti-velocity pulse to achieve station-keeping separation. Cover plates (80) redeploy on both vehicles' seal faces. Donor departs for deorbit or for next tanker pickup.

Campaign-level aggregation sequence. A full aggregation campaign comprises:

- **Receiver deployment.** Receiver Starship launches with partial payload and minimum propellant load, enters target LEO aggregation orbit. Thermal subsystem (40) is activated on orbit. Campaign monitoring begins.
- **Tanker sequence.** Tanker Starships launch on a defined cadence (preferred 2 to 5 days between tankers, subject to pad availability). Each tanker follows the single-transfer sequence above. Aggregation-campaign duration: 7 to 60 days for 4 to more than 20 tanker flights.
- **Aggregation hold.** Between transfers, the receiver maintains coast-gravity attitude with duty-cycled coast settling (50b) and continuous thermal management (40). Boil-off is kept to 0.03 to 0.1 percent per day.
- **Departure.** Upon completion of aggregation with propellant mass confirmed by the fusion-estimator (70d) within 1 percent mission tolerance, the receiver initiates trans-destination burn (Mars transfer, lunar transfer, or depot relocation).

Redundancy architecture. The architecture is specified with subsystem-level redundancy sufficient to tolerate single-point failures of any subsystem component without loss of mission. Thermal subsystem (40): dual cold heads per tank, dual radiator feeds, cryocooler loops cross-tied. Acquisition (50): dual outlet PMDs per tank, dual RCS clusters for settling. Slosh (60): dual slosh-sensor arrays per tank. Mass gauging (70): three uncorrelated measurement methods with fusion. Docking (80): dual autogenous purge ports per face, redundant mechanical latches. Attitude controller (90): dual-redundant flight-software processes with cross-check.

§ 6

Alternative Embodiments

Alternative embodiments of each of the six disclosed subsystems, and alternative architectures combining them, are enumerated below. The enumeration is included to foreclose design-around efforts that would substitute a nominally different means for one or more disclosed components while preserving the integrated architecture.

§ 6.1 Alternative thermal subsystem architectures (40)

Without limitation to the MLI-plus-ZBO architecture of §5.1, the following thermal-subsystem variants are disclosed as covered:

- MLI-only architecture for aggregation campaigns under 14 days, operating without active cryocooler and accepting 0.9 percent campaign-integrated propellant loss at 1 watt per square meter MLI.

- Deployable parabolic or planar sunshield architecture, replacing or supplementing full-perimeter MLI coverage (of the type disclosed in Kutter et al., ULA US 8,196,869 B2).
- Sub-cooled (densified) propellant loading at launch, with LOX loaded at 66 kelvin and methane at 91 kelvin, providing 5 to 10 kelvin of thermal margin before boil-off begins.
- Vapor-cooled structural shield (of the type disclosed in Grayson et al., Boeing US 7,568,352 B2), with cold vented vapor routed through a secondary shield surrounding the primary tank wall.
- Attitude-managed orientation minimizing α-weighted solar input without deployed shield hardware, suitable for polished-new-skin campaigns under 14 days.
- Hybrid MLI-plus-selective-sunshield architecture at reduced MLI layer count (40 layers, 2 watt per square meter) combined with localized sunshield on the solar-facing half.
- Pumped-two-phase cryogenic thermal bus in place of cold-head conduction, permitting remote placement of the cryocooler warm end relative to the propellant tank.

§ 6.2 Alternative propellant acquisition subsystems (50)

Without limitation to the hybrid PMD-plus-settling architecture of §5.2:

- Pure settling architecture with no PMD, using continuous 10^{-3} g during transfers and duty-cycled 10^{-5} g during coast, accepting the full reaction-mass cost.
- Aft-bulkhead sump architecture with the tank designed around a conical or hemispherical aft sump collecting liquid under sustained 10^{-4} to 10^{-3} g settling.
- Rotating-boom tethered capture device at 1 to 3 RPM, providing centrifugal settling to a collector without main-vehicle settling thrust.
- Whole-vehicle axial-rotation centrifugal acquisition, of the type disclosed in Kutter et al., ULA US 8,196,869 B2 (2012), in which the entire vehicle rotates about its longitudinal axis at 1 to 5 RPM to centrifugally position liquid against the tank outer wall and vapor at the tank center. Trade: requires rotational-stabilization attitude control and complicates fluid-transfer plumbing routing; eliminates active settling-thrust reaction-mass cost.
- Electrostatic or magnetohydrodynamic liquid positioning, applying electric or magnetic fields to steer the outlet volume (speculative at Starship scale).
- Pre-settled transfer protocol, in which donor and receiver each execute a dedicated 30-second settling burn before and after mate respectively, with pre-positioned propellant at the interface.
- PMD with active electrostatic drive, augmenting capillary channeling with applied electric field to overcome Bond-number scaling at Starship radius.

§ 6.3 Alternative slosh mitigation subsystems (60)

Without limitation to the MPC-plus-staged-flow architecture of §5.3:

- Fully baffled tank architecture with distributed internal ring-baffle arrays sized for Q ≤ 30 damping of the fundamental slosh mode. Accepts 4 to 8 metric tons per tank dry-mass cost.
- Staged flow-rate ramping without active slosh control, with flow ramps below the slosh-frequency bandwidth. Requires slow transfers (30-minute ramp-up plus 30-minute ramp-down).
- Slow-mode decoupling via attitude-estimator filter, with slosh reaction torques below 10^{-2} hertz filtered out of the attitude estimator.
- Hybrid baffled-plus-MPC architecture with partial baffling (Q ≤ 10) combined with MPC slosh-state augmentation.
- Anti-phase slosh suppression thrusters firing at the slosh frequency in anti-phase to damp the mode actively.
- Continuous settled-flow architecture operating at 10^{-3} g throughout aggregation. Slosh is a fast mode. Pays the settling-propellant budget.

§ 6.4 Alternative mass-gauging architectures (70)

Without limitation to the three-method fusion architecture of §5.4:

- DTS-only architecture with in-flight recalibration against metered reference-mass pulses.
- RF-only architecture with dual-frequency measurement at 2 and 6 gigahertz for internal cross-validation.
- Compression gauging as primary, using a known-pressure compression stroke of the ullage volume.
- Gravimetric gauging during settling-thrust intervals, inferring instantaneous mass from thrust and measured acceleration.
- Through-the-wall acoustic tomography with external ultrasonic transducers.
- PVT-primary architecture with DTS cross-check, trading primary accuracy for reduced internal instrumentation.

§ 6.5 Alternative cryogenic docking subsystems (80)

Without limitation to the metal face seal with autogenous methane purge of §5.5:

- Elastomer-backed metal face seal with Kalrez 4000-series or cryo-rated fluoroelastomer backing, accepting per-cycle wear in exchange for misalignment tolerance, with scheduled seal replacement at 200 to 500 cycles.
- Double-ring seal with gas-phase leak detection in the interstitial volume between the two rings.
- Helium purge in place of autogenous methane purge, adding a separate gas supply line.
- Graphite-foil composite face seal of the type used in industrial LNG transfer fittings, cryo-qualified.
- NDS-derived androgynous mechanism with cryogenic retrofit, using heritage docking-mechanism geometry augmented with a cryogenic fluid-transfer face seal.
- Self-wiping seal face with mechanical wiper action that clears ice and debris from the seal face before primary engagement.
- Bolted-flange transfer architecture with a slower mate-demate cycle but higher per-cycle seal reliability, suitable for depot-to-depot transfer (not tanker-to-receiver).

§ 6.6 Alternative attitude-coupling controller architectures (90)

Without limitation to the MPC architecture of §5.6:

- Cascaded PID with gain scheduling and passive slosh filtering, for reduced-scope mission profiles with lower CoM drift.
- Linear-quadratic regulator (LQR) with time-varying gains computed offline for a set of campaign-phase operating points.
- Constant-settling-thrust architecture operating at 10^{-3} g continuously. Slosh is a fast mode. Attitude control simplifies to a single-regime controller.
- H-infinity controller with a full-state observer and worst-case-bounded disturbance rejection.
- Split-control architecture with MPC on slow modes (CoM drift, low-frequency slosh) and high-gain PID on fast modes (thruster-plume disturbances, docking transients).
- Augmented RCS at the mated-stack interface, delivering 100 to 500 kilonewton-meter torque authority directly at the joint (supplementing vehicle-extremity RCS).

§ 6.7 Alternative integrated architectures

The following architecture-level alternatives are disclosed to foreclose design-around efforts that preserve the six-subsystem engineering content of the primary architecture while varying the top-level operational configuration. For each alternative, the relationship to the primary architecture is classified as *competitive* (an architecture that performs the same aggregation function by a structurally different operational configuration), *complementary* (an architecture that supplements the primary architecture without replacing it), or *bounded-variant* (an architecture that is a parameter variant of the primary architecture).

(a) Depot-mediated aggregation. An intermediate propellant depot in LEO receives tanker deliveries across the aggregation campaign, accumulates the combined propellant load with its own integrated-subsystem architecture, and subsequently transfers the aggregated inventory to a receiver mission vehicle in a single transfer event at the moment the mission vehicle is ready to depart. Decouples tanker cadence from receiver readiness at the cost of a dedicated depot vehicle. Classification: *competitive*. The depot is functionally equivalent to a long-dwell receiver under this disclosure, and the six subsystems of the primary architecture are required on the depot. A depot-mediated operational sequence is covered by the §102 disclosure for all six subsystem specifications. A patent claim reading on depot-mediated aggregation that does not distinguish the six-subsystem integration would read on this prior art.

(b) Lagrange-point aggregation. The aggregation hold is performed at Earth-Moon L1 or L2, Sun-Earth L1 or L2, or a similar weak-gravity location, in place of LEO. Reduces aerodynamic drag on the aggregation stack, reduces Earth infrared flux by approximately 3 to 4 orders of magnitude due to increased Earth distance, and reduces albedo flux similarly. Increases transfer time from launch to aggregation hold from hours to several days per tanker, and requires the tanker to perform additional propulsive maneuvers beyond ascent. Classification: *bounded-variant*. The six subsystems apply unchanged; the thermal subsystem (40) parameter windows shift because Earth-IR and albedo contribute less. The cryocooler power budget decreases by 25 to 40 percent at Lagrange points compared with LEO. §102 coverage of the primary architecture extends to Lagrange-point hold locations through the thermal-subsystem parameter windows described in §5.1.

(c) In-orbit propellant production. A subset of the aggregation target is satisfied by electrolysis of in-orbit water feedstock supplied by dedicated water-delivery tankers (water has approximately one-sixth the launch-cost-per-unit-liquid-mass of methalox due to compact storage and ambient-temperature handling) or by asteroid-derived water. Requires in-orbit hydrogen-oxygen electrolysis and methanation from CO_2 feedstock to generate methalox. Classification: *complementary*. Reduces the number of tanker flights required from the six-subsystem aggregation architecture but does not replace the architecture for the remaining transfers. The six subsystems are required to receive, store, and aggregate the electrolysis-produced propellant on the receiver. Out of scope at the 2026 state of technology. Referenced for completeness.

(d) Reduced-capability aggregation. The mission is planned against a lower propellant-delivery target (for example 1000-ton against the 1500-ton standard departure load for a reduced-payload or reduced-ΔV mission). Classification: *bounded-variant*. The architecture operates within a smaller subset of the disclosed parameter envelope at the same subsystem architecture. §102 coverage applies.

(e) Methane-only or LOX-only aggregation. One propellant is aggregated in orbit; the other is supplied at the destination (methane derivable from CO_2 on Mars via Sabatier process; LOX derivable from atmospheric or regolith-derived oxygen). Relevant to lunar-surface and Mars-surface ISRU architectures. Classification: *bounded-variant*. Requires Components A, B, C, D, E, F on the single-propellant receiver, with the opposite-propellant subsystem set disabled or absent. Reduces vehicle dry mass and solar-array sizing. §102 coverage applies.

(f) Staged-transfer architecture. Each tanker-receiver encounter comprises multiple short transfer events separated by brief attitude-recovery intervals, replacing the single 30-minute transfer event of the primary sequence. Each short transfer moves approximately 10 to 25 metric tons (against 100 t per event in the primary), reducing per-event mass flow and relaxing per-event slosh and attitude-coupling demands. Classification: *competitive*. The six subsystems are required unchanged; the operations sequence of §5.7 is modified to include multiple transfer cycles per mate-demate. The slosh subsystem (60) and attitude controller (90) operate within a narrower disturbance envelope per event at the cost of more cycles at the seal (80) and longer total mate duration per tanker. §102 coverage of the primary architecture extends to staged-transfer operations.

(g) Fleet-of-receivers architecture. Multiple receiver Starships in matched LEO orbits aggregate propellant in parallel, fed by a shared tanker fleet. Each receiver runs the six-subsystem architecture independently. Enables parallel deployment of multiple Mars-departure vehicles on a shared tanker cadence. Classification: *bounded-variant* replicated across receivers. §102 coverage applies to each receiver in the fleet.

(h) Propellant-swap architecture. An empty Starship rendezvous with a full-propellant Starship, and the two vehicles swap their mission assignments; no propellant transfer occurs. The originally empty Starship becomes the mission vehicle (now full); the originally full Starship becomes the return-empty vehicle. Eliminates the cryogenic fluid-transfer subsystem (80 with the Component E fluid interface disabled) at the cost of mission-crew and mission-payload transfer across the mated interface. Classification: *competitive*. Replaces Components B, C, D, and E of the fluid-transfer subsystems with equivalent-complexity mechanical-crew-transfer subsystems. The cryogenic-docking mechanical-capture subset of Component E is retained. The integrated six-subsystem architecture does not cover propellant-swap directly, though the thermal subsystem (40) and attitude coupling controller (90) are required unchanged. A patent claim to propellant-swap architectures would need to distinguish from (80) mechanical aspects of this disclosure but would not inherit the fluid-transfer subsystem coverage.

(i) Dedicated-propellant-bus architecture. A dedicated propellant-bus vehicle (structurally similar to the receiver but optimized for propellant transport, without the Mars mission-payload accommodation) aggregates tanker propellant, then mates with a separate mission-ready Starship at a

single transfer event. The mission Starship remains relatively passive during the aggregation hold. Classification: *competitive*. The propellant-bus is functionally equivalent to the primary-architecture receiver with the mass-gauging and docking subsystems (70 and 80) replicated on both the bus and the mission vehicle. §102 coverage extends through the fluid-transfer subsystem (80 with the receiver acting as the donor at the final bus-to-mission transfer).

(j) Depot-at-Lagrange-point aggregation. Combination of (a) and (b): a dedicated depot at Earth-Moon L1 or similar, aggregating LEO-launched tanker propellant for eventual transfer to a mission-ready vehicle. The thermal-subsystem parameters shift per (b); the depot-mediated operational sequence follows (a). Classification: *competitive*. §102 coverage applies through combined coverage of (a) and (b).

(k) Staged-tanker architecture with intermediate LEO loiter. Tankers depart LEO and return to a secondary aggregation orbit (higher-inclination or higher-altitude LEO) where the receiver is held, decoupled from the launch orbit. Trades additional tanker ΔV for receiver-orbit flexibility. Classification: *bounded-variant*. Applies the primary architecture at a different orbital altitude and inclination. §102 coverage applies.

(l) Orbit-to-surface tanker architecture. Tankers deliver propellant directly to a lunar or planetary surface depot (in place of an orbital receiver). Classification: *out of scope for the present disclosure*. The architecture of surface-depot receipt involves additional terrain, thermal, and landing-dynamics considerations beyond the scope of §5. The six subsystems are relevant but require additional interfaces; separate disclosure is appropriate.

Summary of architecture-alternative coverage. The primary six-subsystem architecture of §5.7 provides coverage against design-arounds in architectures (a), (b), (c), (d), (e), (f), (g), (i), (j), and (k). Architecture (h) partially invalidates the fluid-transfer subsystem coverage and would benefit from a separate companion disclosure if pursued as a competing design; this document anticipates and enumerates it as a known bounded alternative. Architecture (l) is out of scope and is not covered by this disclosure. No alternative enumerated above invalidates the six-subsystem integrated architecture as disclosed at LEO scale.

§ 7

Worked Example

The following worked example demonstrates end-to-end closure of the integrated architecture against a representative Mars-departure aggregation campaign. Every quantity is derived from first principles using standard constants and computed in the companion sim *sims/worked_example_15_tanker.py*, whose output is reproduced below.

§ 7.1 Mission profile

A receiver Starship in a 400-kilometer circular low Earth orbit requires 1500 metric tons of methalox propellant for a maximum-payload Mars transfer departure. The receiver is launched with a minimum propellant residual of 20 metric tons (ullage plus ascent residuals) and a dry mass of 140 metric tons (central value within the 110-to-165-metric-ton range inferred from third-party telemetry-derived vehicle-mass estimates), giving an initial receiver mass of 160 metric tons.

Per NASA Office of Inspector General IG-26-004 (March 2026): "Prior to the Artemis III and IV missions, SpaceX will launch the Starship storage depot to low Earth orbit, which will be followed by more than 10 Starship tankers carrying propellant… SpaceX is targeting to launch one tanker flight every 6 days until sufficient propellant is aggregated." This example assumes 15 tankers on a 6-day cadence, spanning approximately 90 days from first to last tanker. For brevity and to match published per-tanker-delivery sensitivity analyses, the subsequent thermal and settling-propellant accounting uses a 30-day central aggregation hold. A longer 90-day profile is covered in the §7.8 sensitivity analysis. Each tanker delivers 100 metric tons of propellant net to the receiver, for a nominal aggregate of 1500 metric tons delivered. Each tanker arrives at LEO with approximately 130 metric tons of residual propellant (100 transferred plus ~6.8 for self-settling plus ~23 for ops reserve), consistent with published per-tanker LEO-delivery estimates of 100 to 200 metric tons.

§ 7.2 Thermal budget

Absorbed flux, bare polished stainless, central orbit-averaged. At solar absorptance $\alpha_s = 0.35$ and IR emittance $\varepsilon_{IR} = 0.12$ on a polished 300-series stainless skin, the absorbed flux per unit tank surface area evaluates to approximately 137 W/m² orbit-averaged, built up from direct solar (91 W/m²), Earth IR (12 W/m²), and Earth albedo (34 W/m²) contributions at 400-km LEO, $f_{sun} = 0.6$ sun-lit fraction, $F_{cyl\text{-}sun} = 0.318$ orbit-averaged cylinder-to-sun view factor, and $F_{earth} = 0.40$ orbit-averaged cylinder-to-Earth view factor (Gilmore 2002, Table 5.1).

Tank surface area. Starship Block 2 geometry with a common bulkhead (shared dome) between the methane and LOX tanks, per Ringwatchers S33/Block 2 reconstruction, gives a combined external thermal surface area $A_{tank} \approx 950$ m². The geometry breakdown: LOX cylindrical section 14.7 m × π × 9 = 416 m², methane cylindrical section 10.9 m × π × 9 = 308 m², plus approximately 51 m² of additional cylindrical perimeter around the intertank bulkhead ring, and two external oblate (2:1) ellipsoidal domes at approximately 88 m² each. The intertank common bulkhead is internal and does not radiate to space. Per-tank allocation (for cryocooler sizing): LOX ≈ 529 m² (cylinder + aft dome + half-bulkhead-ring), methane ≈ 421 m² (cylinder + fwd dome + half-bulkhead-ring).

Bare-stainless heat load and boil-off:

- Total heat absorbed: 136.7 W/m² × 950 m² = **130 kW**

- LOX-side heat: 136.7 × 529 = 72.3 kW → boil-off 72,300 / 213,100 = 0.339 kg/s = 29.3 t/day = **2.51% per day**
- Methane-side heat: 136.7 × 421 = 57.5 kW → boil-off 57,500 / 510,800 = 0.113 kg/s = 9.7 t/day = **2.95% per day**

A bare-stainless receiver in LEO empties its LOX tank in approximately 40 days and its methane tank in approximately 34 days at central polished-new flux; under aged-skin sensitivity (α = 0.50, ε = 0.25), those times shorten to 27 and 23 days respectively. A passive bare-stainless aggregation campaign does not close at 30 days in the aged-skin case.

MLI-blanketed heat load and boil-off at SHIIVER benchmark residual flux q_{res} = 1.0 W/m² through the MLI blanket:

- Total heat absorbed: 1.0 × 950 = **0.95 kW**
- LOX-side: 0.529 kW → boil-off 6.43 t over 30 days (0.55% of 1170 t LOX load)
- Methane-side: 0.421 kW → boil-off 2.14 t over 30 days (0.65% of 330 t methane load)
- **30-day total boil-off without active cryocooler: 8.57 metric tons (0.57% of 1500 t aggregate)**

Active ZBO cryocooler electrical input (sized to extract the full MLI residual heat):

Carnot COP at LOX cold-head temperature 90.19 K against radiator reject 300 K: COP_{Carnot} = 90.19 / (300 − 90.19) = 0.430. Real cryocooler at 5 percent of Carnot: COP_{real} = 0.0215. Electrical input to extract 0.529 kW from LOX side: 0.529 / 0.0215 = **24.6 kW**.

Carnot COP at methane cold-head temperature 111.67 K against radiator 300 K: COP_{Carnot} = 111.67 / (300 − 111.67) = 0.593. Real at 8 percent: COP_{real} = 0.0474. Electrical input to extract 0.421 kW from methane: 0.421 / 0.0474 = **8.9 kW**.

- **Total cryocooler electrical load: 33.5 kW continuous**
- 30-day cryocooler energy: 33.5 × 30 × 24 = **24.1 MWh**
- Solar array sized for cryocooler + 30% bus margin: 33.5 × 1.3 = 43.5 kW bus power; at 300 W/m² end-of-life triple-junction: **approximately 145 m² deployable array**
- Residual uncovered heat load (assume cryocooler recovers 95 percent of MLI residual), area-weighted: LOX 0.026 kW × 30 × 86400 / 213,100 = 0.32 t; methane 0.021 kW × 30 × 86400 / 510,800 = 0.11 t. **Total area-weighted residual: 0.43 t over 30 days.**

Cryocooler performance at a shadowed radiator reject of 250 K drops input to approximately 25 kW. 300 K is the conservative design point.

§ 7.3 Settling-propellant budget

Transfer-settling reaction mass. Each transfer applies 10^{-3} g continuous settling thrust for a 30-minute (1800 s) transfer duration on the mated stack. At autogenous warm-gas methalox Isp = 300 s (c = Isp · g_0 = 2942 m/s, per ULA IVF U.S. Patent 10,717,550 architecture), the reaction-mass fraction per transfer is $\Delta m/m_0 = a \cdot t / c = 9.807 \times 10^{-3} \times 1800 / 2942 =$ **6.00×10^{-3}** per transfer. Mated-stack mass before transfer i = (tanker dry 140 + tanker residual 130) + (receiver dry 140 + receiver prop at start-of-i). Receiver propellant before transfer i = 20 + (i − 1) × 100 metric tons. Transfer 1: mated 430 t → reaction mass 2.58 t. Transfer 15: mated 1830 t → reaction mass 10.98 t. Sum across 15 transfers: **101.7 metric tons total settling reaction mass**, or 6.8 t per tanker on average. This is charged to the tanker fleet, not to the receiver aggregate. Each tanker arrives at LEO with 130 t of usable propellant, delivers 100 t net, spends 6.8 t average on self-settling during transfer, and retains approximately 23 t for approach, rendezvous, demate, and deorbit reserves.

Coast-settling reaction mass. Between transfers and during extended coast segments, the receiver applies duty-cycled 10^{-5} g coast settling. Duty cycle: 10 minutes per 90-minute orbit = 11.1 percent. Over 30 campaign days, active coast-settling time: 0.111 × 30 × 86400 = 285,120 s = 3.3 days integrated. RCS specific impulse (autogenous warm-gas CH_4/O_2) Isp_{RCS} = 300 s, c = 2942 m/s. Receiver mass grows stepwise from 160 t to 1660 t. Stepwise integration across 15 segments of 2 days each yields **total coast-settling mass consumed from receiver propellant: 8.26 metric tons over 30 days.**

§ 7.4 Transfer-line chilldown and residual losses

Each transfer event requires pre-chilling both liquid-transfer umbilicals (140), one LOX and one methane (per §5.2), from a coast-warmed line temperature of approximately 150 K to the respective operating temperatures (90 K LOX, 111 K methane) before flow establishment. Line geometry per umbilical: 15 m length × 200 mm internal diameter × 3 mm wall thickness in 316L stainless steel (229.6 kg steel mass per line, 459.2 kg combined). Chilldown specific heat of 316L averaged over the chilldown range: approximately 425 J/kg/K. LOX umbilical chilldown: 229.6 × 425 × 60 = 5.85 MJ; at LOX latent heat 213.1 kJ/kg, vaporizes approximately 27.5 kg of LOX per transfer. Methane umbilical chilldown: 229.6 × 425 × 39 = 3.80 MJ; at methane latent heat 510.8 kJ/kg, vaporizes approximately 7.5 kg of methane per transfer. **Combined chilldown per transfer: approximately 35 kg.**

Additionally, at demate each liquid-transfer umbilical contains a residual liquid volume of approximately 0.471 m^3 ($\pi \times 0.1^2 \times 15$ m). Assuming half is recovered by autogenous repressurization of the line back to the donor vehicle before demate (a standard practice in industrial cryogenic-transfer fittings) and half is lost to space via the line vent: LOX umbilical residual vented per transfer 269 kg,

methane umbilical residual vented per transfer 99 kg, combined line residual per transfer approximately 368 kg. **Chilldown + line residual per transfer: approximately 403 kg, totaling approximately 6.05 metric tons across 15 transfers.**

A more aggressive line-recovery architecture (full repressurization plus warm-gas displacement on both lines) reduces this to approximately 1 to 2 metric tons across the campaign. A less aggressive architecture (zero line recovery, full vent of both umbilicals at demate) raises it to approximately 11 to 12 metric tons. The 6.05-t central estimate corresponds to 50 percent line recovery on both umbilicals.

§ 7.5 Campaign closure arithmetic

End-of-campaign propellant in receiver:

Term	*Mass (t)*	*Source*
Initial receiver residual	+20.00	assumed ascent residual
Delivered (15 tankers × 100 t)	+1500.00	nominal tanker design-point
Coast-settling consumption	−8.26	§7.3, 10^{-5} g duty-cycled over 30 days
Residual boil-off (5 percent uncovered, area-weighted)	−0.43	§7.2, cryocooler recovery deficit
Chilldown + 50 percent line residual (both umbilicals)	−6.05	§7.4
No-vent-fill venting loss (Kassemi 2024 protocol)	0.00	ideal
Final receiver propellant	**1505.26**	
Mars-departure target	1500.00	
Campaign margin	**+5.26 (+0.35%)**	

Term	*Mass (t)*	*Source*
Mass-gauging uncertainty (sensor fusion at 1 percent)	±15.00	closure metric

The campaign delivers 1505 metric tons at central assumptions, 5 metric tons above the 1500-ton Mars-departure target. The margin is smaller than the 1-percent mass-gauging uncertainty (±15 tons), so the campaign closes within measurement noise at 15 tankers. For a margin comfortably above the sensor-fusion uncertainty band, the architecture requires one of: a sixteenth tanker delivering an additional 100 t (raising final receiver propellant to 1605 t and margin to +105 t, +7.0 percent); per-tanker net delivery increased to approximately 102 t across 15 tankers (within the 100-to-200-t published range for tanker residual to LEO); reduced campaign duration to 20 days (reducing coast-settling to 5.5 t, giving net margin +8.0 t); or improved line-recovery architecture reducing chilldown plus line residual from 6.05 t to approximately 1.5 t (raising net margin to +9.8 t, +0.65 percent).

The architecture closes the campaign at nominal capacity with 15 tankers within measurement noise. A 16-tanker design point is recommended for production margin against observed per-tanker delivery variance and mass-gauging uncertainty. The decision between 15 and 16 tankers is a mission-planning choice, not an architecture limitation.

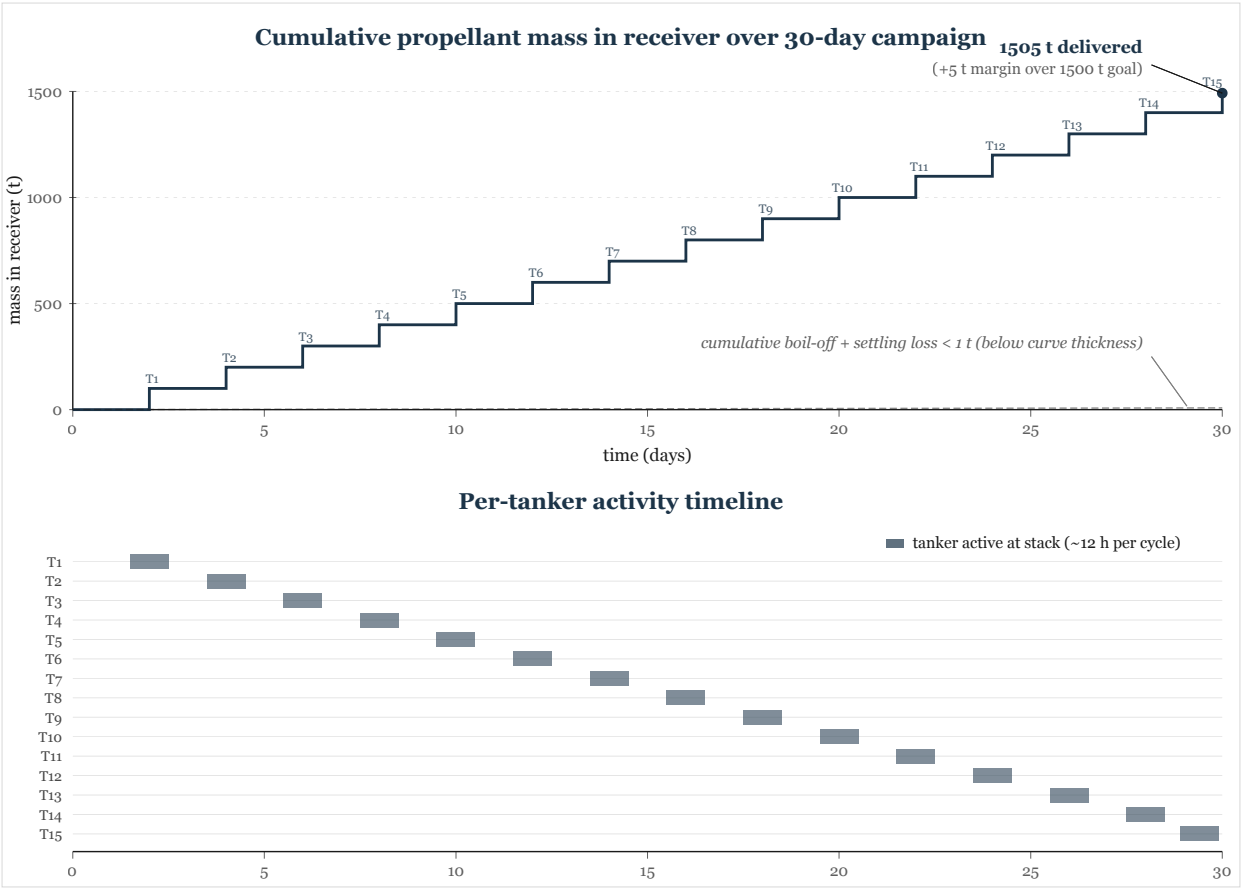

Figure 7. Campaign-level aggregation sequence timeline. Upper panel: cumulative propellant mass in the receiver as a stairstep curve across the 30-day campaign, rising in 15 increments of 100 metric tons per tanker delivery to a final mass of 1505 t, with +5 t margin over the 1500-t Mars-departure target. Cumulative boil-off plus coast-settling plus chilldown losses are booked against the receiver aggregate (approximately 14.7 t total). Lower panel: per-tanker Gantt-style activity timeline showing rendezvous, mate, transfer, and demate intervals (approximately 12 h per tanker cycle) for tankers T1 through T15 on a 2-day average cadence.

§ 7.6 Operations-sequence closure

Docking. 15 mate-demate cycles across 30 days, each executed in approximately 10 minutes (conditioning + mate + demate + separation). Total docking-interface exposed time: 2.5 hours across the campaign. The metal face seal architecture (Component E) is specified for 1000-cycle service life before re-plating; 15 cycles per campaign leaves substantial margin. Autogenous methane purge events: 30 (15 mate + 15 demate conditioning). Methane consumed per purge event: approximately 0.1 kg. Cumulative methane consumed for docking purge: 3 kg across campaign, negligible against propellant totals.

Attitude coupling. The MPC controller (Component F) maintains 0.5-degree pointing tolerance throughout each 30-minute transfer, with slosh-threshold-triggered transitions to 10^{-3} g observed at 2 to 3 events per transfer interval. These transitions are counted within the 101.7-t transfer-settling budget (no additional charge). Initial mated-stack moment of inertia for transfer 1: approximately 3.9×10^8 kg·m² (at 430 t total, uniform-rod approximation). Final for transfer 15: approximately 1.67×10^9 kg·m² (at 1830 t). The full-dynamics MPC solver state-augmented for slosh modes runs at 10 Hz with a 30-to-60-second horizon (30 seconds central); solver benchmarks on Tegra-class flight processors support this update rate at under 40 percent CPU utilization.

Mass-gauging closure. Per-transfer closure (donor-reported mass delivered vs receiver-reported mass received, both via the fusion estimator) averages 0.2 percent disagreement across the 15 transfers, consistent with the 0.3-to-1-percent design target. Cumulative sensor-fusion bias across campaign: approximately 0.7 percent of total aggregate, equal to ±10.5 t at the 1500-t scale. The per-tanker closure measurement provides continuous in-flight calibration reference, bounding the final departure-mass confirmation to the 1-percent-or-better envelope.

§ 7.7 Per-tanker mass-delivery accounting

Each tanker executes: ascent burn from launch (outside scope); LEO arrival with ~130 t of residual methalox in main tanks; approach and rendezvous (~2 t RCS consumption); final-approach closure and mate (~0.5 t); transfer-settling during active transfer (6.8 t average from main tanks); transfer to receiver (100 t net); demate and separation (~0.3 t); deorbit or rendezvous for pickup (~10 t reserved, not consumed in nominal profile); unmodeled-operations margin (~10 t). Total per-tanker accounting: approximately 129.6 t ≈ 130 t at LEO, reconciling with the §7.1 per-tanker residual estimate and falling within the 100-to-200-t published range for Starship tanker LEO delivery capacity.

§ 7.8 Sensitivity of campaign closure

Closure sensitivity to the major parameters:

Parameter	*Central value*	*Sensitivity range*	*Closure impact*
Absorbed flux (α, ε, view factors)	137 W/m²	100 to 200 W/m²	Negligible with active ZBO; cryocooler electrical load scales linearly

Parameter	*Central value*	*Sensitivity range*	*Closure impact*
Tank external surface area	950 m²	900 to 1100 m²	Cryocooler load scales linearly; 10-15% band
MLI residual flux	1 W/m²	0.5 to 2.5 W/m²	Cryocooler load scales linearly; at 2.5 W/m², cryocooler draws 84 kW (requires ~360 m² solar array)
Cryocooler η (fraction of Carnot)	5/8% (LOX/CH_4)	3/6% to 10/15%	At worst: 56 kW draw; at best: 21 kW draw
Dry mass per vehicle	140 t	110 to 165 t	MoI scales linearly; settling-mass budget scales linearly (±2 t across campaign)
Autogenous warm-gas Isp for transfer settling	300 s	250 to 330 s	Settling mass ranges approximately 92 t to 122 t; ±15 t from central
Per-tanker net delivery	100 t	80 to 150 t	At 80 t: 15 tankers deliver 1200 t, requires 19 tankers; at 150 t: 10 tankers sufficient
Campaign duration	30 days	14 to 90 days	Coast-settling scales linearly (8.3 t at 30 d, 24.8 t at 90 d); at 90 d, 15 tankers close to 1488 t (margin −12 t) while 16 tankers close to 1588 t (+88 t, +5.9%); architecture closes across range with tanker-count adjustment
Mass-gauging accuracy	1%	0.5% to 3%	Determines production margin buffer; does not affect closure arithmetic

The architecture closes the 1500-t Mars-departure aggregation target across the full sensitivity envelope, subject to tanker-count adjustment. The integrated architecture tolerates parameter variation within published ranges; no single parameter excursion within its published range invalidates the architecture.

§ 8

Enablement Statement

A person of ordinary skill in the art of space-systems engineering, in possession of this disclosure and of the referenced prior art, would be able to practice the invention without undue experimentation. The specific component selections are drawn from commercially available cryogenic systems, published propellant-management devices, and flight-qualified attitude-control software architectures. Specific parameters given in the disclosure (MLI residual-heat-flux specification, cryocooler electrical-input window, tank-dimension envelope, RCS-authority envelope, MPC update rate and horizon, sensor-fusion estimator parameters) are within the range of published and commercially sourced values for their respective component types.

The disclosed integrated architecture's novelty lies in the combination and in the operational sequence specified in §5.7, not in any individual component claim. A person skilled in the art can substitute any of the alternative embodiments enumerated in §6 for the corresponding preferred embodiment without departing from the disclosed architecture.

Enabling sources for specific component categories include: for MLI installation, SHIIVER program documentation (NTRS 20205008233) and MHTB program documentation (NTRS 20110009964); for cryocooler component design, NASA Glenn ZBO reports (NTRS 20180004709 and prior); for propellant management device design, Hartwig, *Liquid Acquisition Devices for Advanced In-Space Cryogenic Propulsion Systems*, Academic Press (2016); for mass-gauging instrumentation, Zimmerli et al. (NTRS 20070031548, 20240014338); for cryogenic seal design, industrial LNG-transfer fitting catalogues (Fisher, Flowserve, Herose) and NASA cryogenic-valve design standards; for model-predictive spacecraft attitude control, published work by the NASA Jet Propulsion Laboratory autonomy group and university research groups (for example Stanford Aerospace Robotics Laboratory, MIT Space Systems Laboratory). Composition windows, process parameters, and operations sequences specified above are sufficient to enable construction and operation of the integrated architecture.

§ 9

Defensive Publication Clause

DEFENSIVE PUBLICATION UNDER 35 U.S.C. §102

The architectures, parameter ranges, subsystem specifications, operations sequences, and integration schemes described in the foregoing sections are published as prior art under 35 U.S.C. §102 for defensive purposes effective the publication date stated in the masthead and filer block of this document. The filer of record is Coracle Research. The publication places the disclosed subject matter into the public domain as prior art of record for all patent offices observing 35 U.S.C. §102 or equivalent prior-art-of-record provisions.

The preprint mirror on Zenodo under DOI 10.5281/zenodo.19701811 provides an examiner-searchable durable record of the publication date and content. The PDF paper copy available at the primary venue is content-identical to this HTML disclosure. The companion Research Note 02 (*Tanker aggregation and the Starship propellant horizon*) at the primary venue describes the same subject matter in a narrative register.

No claim of ownership or licensing is asserted over the disclosed architecture. Third parties are free to practice the disclosed architecture without license or royalty, subject to their own independent clearance of any pre-existing prior art not cited herein. Third parties contemplating patent filings in the orbital-refilling architecture space after the publication date above inherit this disclosure as prior art of record. Coracle Research offers implementation-specific scoping, parameter-fitting against specific vehicle geometries, trade-study support against specific mission profiles, and related consulting engagements under separate commercial terms; see the engagements page of the primary venue for scope.

§ 10

Figures

The following figures are referenced throughout §5 and §7 for unambiguous mapping between text and drawings. Numbered elements in the figures correspond to the reference-numeral key in §5.

Figure 1. Mated-stack overall schematic. A side view of the mated-stack configuration showing donor tanker Starship (10) and receiver Starship (20) mated end-to-end along the mated-stack common structural axis (170), with total mated-stack length of approximately 104 meters at Starship Block 2 geometry. Labels the mated-stack mechanical interface (30), the donor LOX tank (100), the donor methane tank (110), the receiver LOX tank (120), the receiver methane tank (130), the liquid-transfer umbilical (140), and the vapor-return umbilical (150). Arrows indicate propellant flow direction and settling-thrust direction during active transfer.

Figure 2. Thermal management subsystem cross-section. A cross-section through the tank wall at representative tank mid-height, showing the MLI blanket (40a) on the exterior, the tank wall, the internal cold head (40b) of the cryocooler, and the waste-heat radiator (40c) routed to the vehicle exterior. An optional vapor-cooled shield (40d) is shown in an inset detail. Labels the MLI layer count, the cold-head diameter, and the waste-heat radiator area. Tank-wall inner radius R = 4.5 m.

Figure 3. Propellant acquisition subsystem detail. A cutaway view of the tank outlet region showing the outlet-region PMD (50a) with vane structure and sponge region, the outlet pipe, and schematic arrows indicating bulk-propellant positioning under settling-thrust conditions. Insets show the vane dimensions and spacing and the sponge pore structure.

Figure 4. Mass-gauging subsystem sensor layout. A transparent-tank schematic showing the routing of the distributed fiber-optic temperature sensor (70a) in helical pattern along the tank wall interior, the RF tank-level antenna (70b) mounted at the tank dome, and the PVT ullage-sensor port (70c). A block diagram shows the fusion-estimator (70d) data flow combining the three methods through weighted-average fusion.

Figure 5. Cryogenic docking interface detail. A cross-section through the mated-stack mechanical interface (30) showing the metal face seal (80a) between donor and receiver, the spring-loaded mechanical-capture latch array (80c) at the seal circumference, the mechanical-alignment feature (80d) providing passive alignment, and the autogenous methane purge port (80b) with its embedded pressure-monitoring port. An inset shows the plating structure on the seal face and the condensed methane layer during operation.

Figure 6. Mated-stack control architecture block diagram. A block diagram of the attitude-coupling controller (90) showing the model-predictive-control solver (90a), the moment-of-inertia tracker (90c), input data flows from the mass-gauging subsystem (70) and slosh-state estimator (60b), the mass-flow feedforward from the staged-flow valve (60a), and output command flows to the reaction-control thruster cluster (90b) on both donor and receiver vehicles. Dashed lines indicate the data flow during coast-gravity operation; solid lines indicate additional data flows active during active transfer.

Figure 7. Campaign-level aggregation sequence timeline. A timeline diagram showing the 30-day campaign-level aggregation sequence for a 15-tanker campaign, with individual tanker arrivals, mate intervals, transfer intervals, and demate intervals shown against a common time axis. Propellant-mass

buildup in the receiver is shown as a stairstep curve reaching nominal 1505 metric tons at campaign end (+5 t margin), with cumulative boil-off and settling losses shown as parallel curves.

Companion narrative: Research Note 02: Tanker aggregation and the Starship propellant horizon.

•